P-T evolution of Alpine metamorphism in the southern Aspromonte Massif (Calabria - Italy)

Autor(en): **Ortolano, Gaetano / Cirrincione, Rosolino / Pezzino, Antonino**

Objekttyp: **Article**

Zeitschrift: **Schweizerische mineralogische und petrographische Mitteilungen = Bulletin suisse de minéralogie et pétrographie**

Band (Jahr): **85 (2005)**

Heft 1

PDF erstellt am: **24.04.2024**

Persistenter Link: https://doi.org/10.5169/seals-1652

Schweizerische Mineralogische und Petrographische Mitteilungen 85, 31–56, 2005

P–T evolution of Alpine metamorphism in the southern Aspromonte Massif (Calabria – Italy)

Gaetano Ortolano[1], *Rosolino Cirrincione*[2] and *Antonino Pezzino*[3]

Abstract

The crystalline basement of the southern Calabrian-Peloritani nappe pile edifice (Aspromonte Massif and Peloritani Mountains) consists of several tectonic slices, which were stacked during the Miocene Apennine thrust sheet emplacement (Fig. 1). The two lowermost tectonic slices of this nappe-edifice, here called respectively Aspromonte-Peloritani Unit and Samo-Africo Complex, tectonically overlap along a thick Late Oligocene mylonitic shear zone, which involves both remnants of the Hercynian chain and Alpine metamorphic rocks (Figs. 1–2).

A structural and petrological study was employed to reconstruct both the entire P–T evolution of the two units and the kinematics of orogenic transport, which characterise the Late Oligocene mylonitic stage. P–T estimates were made using an integrated approach derived from conventional thermobarometry, computation of metamorphic equilibria in the NaCaKFMASH system, and an analysis of the deformation behaviour of quartz, feldspar and garnet.

The shear event marks the beginning of the joint structural and metamorphic history. Prior to this event, the two units had undergone very different tectonometamorphic evolutions. The upper unit (Aspromonte-Peloritani Unit) underwent pre-mylonitic HT–LP Variscan polyphase retrograde metamorphism (peak conditions 0.39–0.5 GPa; 650°–675 °C). By contrast, the deeper Samo-Africo Complex underwent pre-mylonitic LT–HP metamorphism (peak conditions 0.98–1.2 GPa; 480°–560 °C), linked to crustal thickening of an Early Alpine age.

Syn-mylonitic P–T estimates confirm the beginning of the joint tectonometamorphic history, evolving from 500° to 350 °C with P ranging from 0.775 to 0.325 GPa. This event, linked to Late Oligocene Alpine shearing, developed during the uplift and exhumation of the crystalline basement rocks along a deep-seated compressional shear zone.

The above results lead us to suggest a new geodynamic scenario for the southern sector of the Calabrian Peloritani Orogen: Following subduction of the Aspromonte-Peloritani Unit and the Samo-Africo Complex these two units were extruded along the collisional suture. In this tectonic reconstruction, the Samo-Africo Complex is interpreted as a post-Variscan sedimentary succession involved in a complete Alpine orogenic cycle, consisting of an Early Alpine crustal thickening stage and a Late Alpine Africa-verging compressional shear stage.

Keywords: Variscan and Alpine metamorphism, P–T path, kinematic indicators, mineral reactions in NaCaKFMASH system, Calabria.

1. Introduction

The Aspromonte Massif and Peloritani Mountains form the southern sector of the Calabrian Peloritani Orogen (CPO), a segment of the Alpine orogenic belt located in the central Mediterranean area and bounded by the Sangineto (north) and Taormina (south) transpressive geological lines (Ghisetti et al., 1991) (Fig. 1a). The actual structure of the CPO is essentially a nappe-pile edifice, involving distinct tectonic slices of metamorphic basement rocks and Mesozoic–Cenozoic sedimentary sequences. The basement units are remnants of both the Hercynian chain and Alpine metamorphic rocks incorporated into the Alpine-Apennine nappe system of the western Mediterranean.

The present-day structure of the CPO is the result of two different evolutionary stages. The first Alpine event (Eocene–Oligocene), characterised by relatively high-pressure metamorphism, is related to a crustal thickening stage, associated with the collision between the Adria promontory and the European plate (Borsi and Dubois, 1968; Pezzino et al., 1990, 1992; Platt and Compagnoni, 1990). The second stage (Late Oligocene to Present) is related to the south-east migration of the CPO, related to slab rollback in the

[1] Dipartimento di Scienze Geologiche, Università degli Studi di Catania, Corso Italia 57, I-95129 Catania, Italy. *Corresponding author:* <ortolano@unict.it>
[2] Dipartimento di Scienze della Terra, Università della Calabria, Via P. Bucci, I-87036 Arcavacata di Rende (CS), Italia. <cirrincione@unical.it>
[3] Dipartimento di Scienze Geologiche, Università degli Studi di Catania, Corso Italia 57, I-95129 Catania, Italia. <pezzino@unict.it>

0036-7699/05/0085/31

Ionian domain as a consequence of the opening of the Tyrrhenian basin (Dewey et al., 1989; Gueguen et al., 1998; Rosenbaum et al., 2002, and references therein).

The origin and geodynamic significance of the CPO is still a matter of debate, with the following principal hypotheses: (a) the CPO is a fragment of the Alpine orogenic belt, belonging to the western

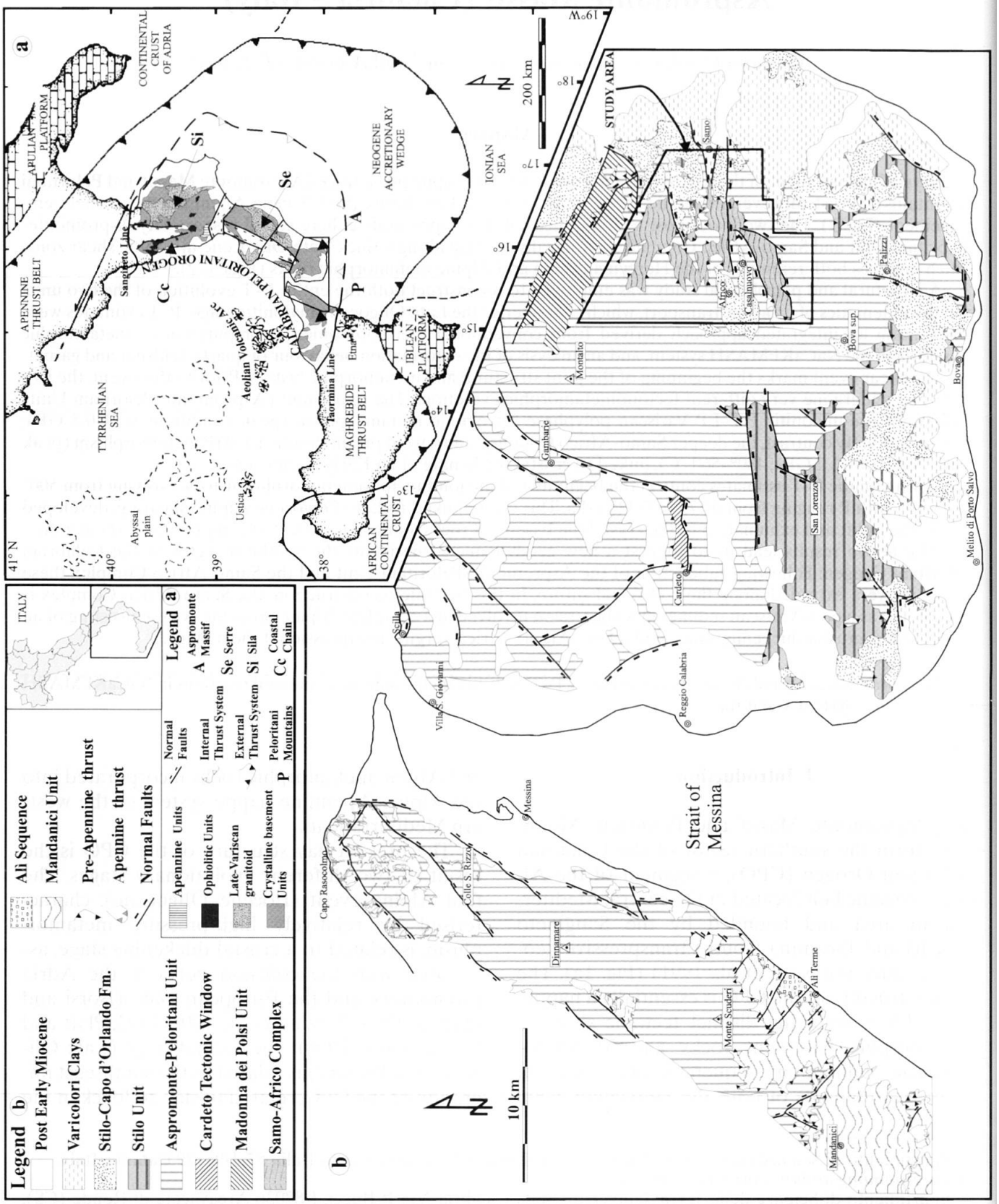

Fig. 1 (a) Geological-structural sketch-map of the south-western Mediterranean area; (b) Geological sketch-map of the southern sector of the Calabrian-Peloritani Orogen and location of study area.

margin of Adria; it was emplaced northwestwards onto Tethyan ophiolites (Late Cretaceous–Paleogene), forming what some authors consider to be a southern extension of the Alpine chain (Alvarez, 1976; Amodio-Morelli et al., 1976). A later back-thrust (directed both east and south) overrode the African continental margin and emplaced the CPO on Apennine domains (Late Oligocene–Early Miocene times); (b) the CPO represents a south-western fragment of the European paleo-margin (Late Cretaceous–Paleogene), was emplaced progressively eastward onto the Adria margin during Miocene times (Ogniben, 1969, 1973; Bouillin, 1984; Bouillin et al., 1986; Dewey et al., 1989; Gueguen et al., 1998; Rosenbaum et al., 2002).

One of the main problems regarding the interpretation of the CPO geological framework is the difficult correlation between the northern tectonic units (northern Calabria, as far as the Soverato-Mesima valley alignment) with those of the southern sector, owing to their different tectonometamorphic evolution (Bonardi et al., 1982; Scandone, 1982; Tortorici, 1983; Dercourt et al., 1985). One of the main differences between the two sectors is that ophiolitic units, characterised by Early Alpine metamorphism varying between 60 and 35 Ma (Schenk, 1980; Van Dijk et al., 2000; Rossetti et al., 2001), are lacking in the south (Fig. 1a). Indeed, the presence, distribution and characterisation of the Alpine metamorphism in the CPO southern sector becomes an important geodynamic constraint in reconstructing the Oligocene scenario of the Calabrian terranes.

Over the last two decades, many authors have documented and variably interpreted the presence of Alpine metamorphism in the CPO southern sector. This is particularly evident in the central Aspromonte Massif, where intense polyphase Alpine reworking has been identified (Bonardi et al., 1987; Pezzino et al., 1990, 1992; Platt and Compagnoni, 1990; Cirrincione and Pezzino 1991; Messina et al., 1992, 1996; Atzori et al., 1994; Puglisi and Pezzino, 1994). It develops in two stages: an early relatively high-pressure stage and a later shear stage, which occurs at lower pressure conditions.

Some authors hold that the early high-pressure stage developed during crustal thickening related to the continental collision between the Adria promontory and the European plate (Pezzino et al., 1990, 1992; Platt and Compagnoni, 1990). By contrast, while Platt and Compagnoni (1990) consider that the later shear stage developed during an extensional regime, related to the exhumation of the orogen during the Late Oligocene–Early Miocene, other authors (e.g., Pezzino et al., 1990, 1992) link the same event to nappe emplacement during a compressional shear stage related to an early Africa-verging collisional event. In this context, the structural and thermobarometric evolution of the CPO southern sector is a key to understanding the geodynamic significance of the Calabrian orogen within the movements of the plate and/or microplates which controlled the evolution of the Late Oligocene–Miocene western Mediterranean scenario.

The present structural and petrological study contributes new information about the Alpine tectonometamorphic evolution of the two lowermost units of the Aspromonte Massif, here called respectively Aspromonte-Peloritani Unit and Samo-Africo Complex (Fig. 1b).

2. Geological setting

The thrust edifice of the CPO southern sector consists of stacked tectonic units with a variable metamorphic evolution. In the Aspromonte Massif, the uppermost unit is made up of low greenschist- to low amphibolite-facies Paleozoic metamorphic rocks, the Stilo Unit (SU) (Crisci et al., 1982; Bonardi et al., 1984; Graeßner and Schenk, 1999). In the study area, it outcrops as sporadic klippen and consists of very low-grade Hercynian metapelites (Figs. 1b–2). The SU lies in brittle tectonic contact over the Aspromonte-Peloritani Unit (APU), which is made up of amphibolite-facies Paleozoic rocks with late to post-Hercynian peraluminous intrusive bodies, locally overprinted by Alpine age metamorphism, which developed at about 25–30 Ma (Bonardi et al., 1987). A thick mylonitic horizon marks the tectonic contact between the APU and several underlying low- to medium-grade tectonic windows, surfacing in the western and central-eastern sectors of the Aspromonte Massif: (a) the Cardeto window (Bonardi et al., 1980a); (b) the Madonna dei Polsi Unit (Pezzino et al., 1990); (c) the Africo Unit (Messina et al., 1992) (Fig. 1b).

The westernmost tectonic window (Cardeto window) and Madonna dei Polsi Unit are made up of a greenschist-facies metapelitic sequence, significantly overprinted by Alpine mylonitic metamorphism. Bonardi et al. (1987), Platt and Compagnoni (1990) and Messina et al. (1992, 1996), believe that the Madonna dei Polsi Unit represents a totally re-equilibrated zone of the APU related to Alpine retrograde tectonometamorphic evolution. By contrast, Pezzino et al. (1990, 1992) believe that the Madonna dei Polsi area corresponds to an underlying prograde HP Early Alpine metamorphic unit (Madonna dei

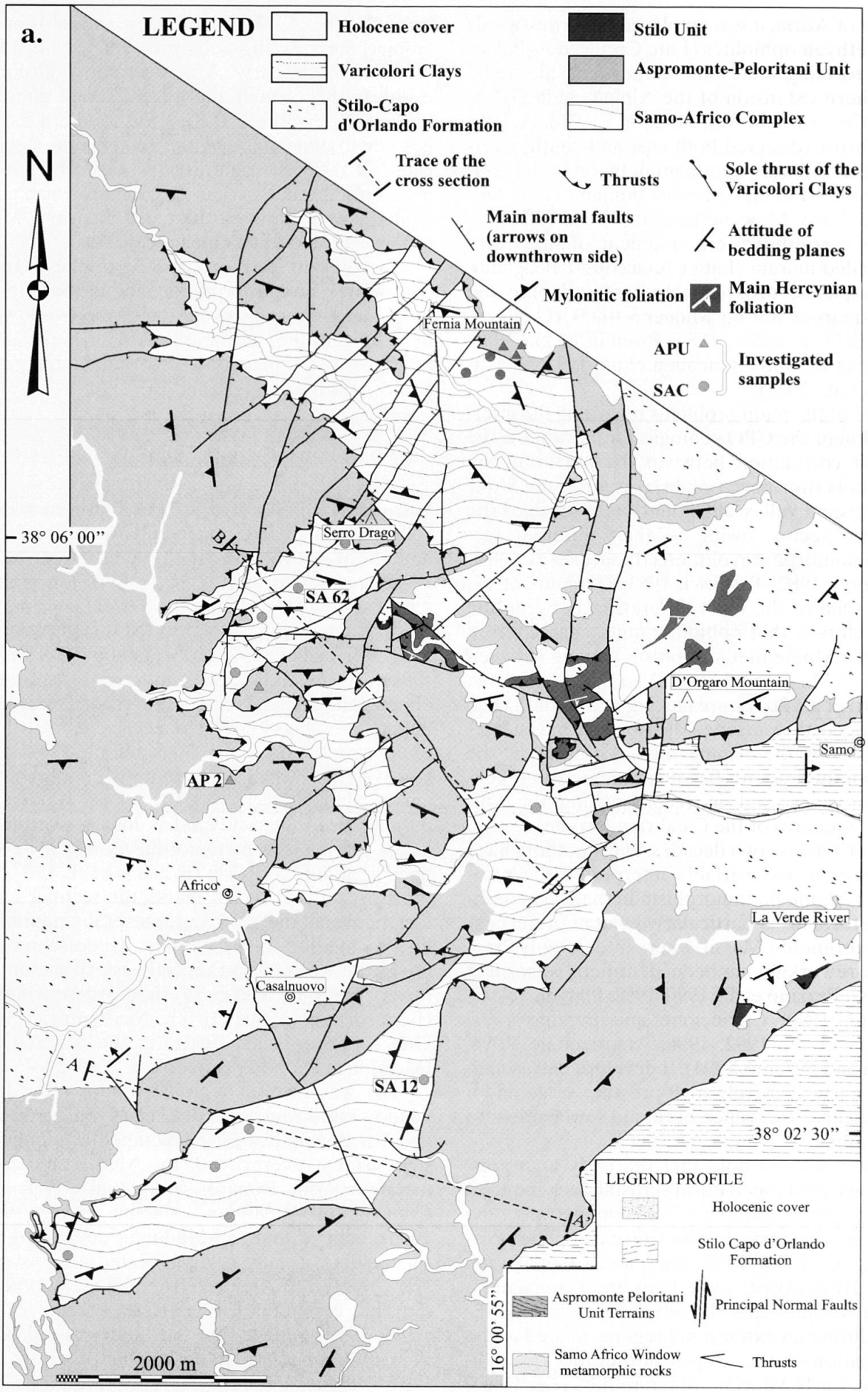
a.
LEGEND
Holocene cover
Varicolori Clays
Stilo-Capo d'Orlando Formation
Stilo Unit
Aspromonte-Peloritani Unit
Samo-Africo Complex
Trace of the cross section
Thrusts
Sole thrust of the Varicolori Clays
Main normal faults (arrows on downthrown side)
Attitude of bedding planes
Mylonitic foliation
Main Hercynian foliation
APU
SAC
Investigated samples
N
38° 06' 00"
Fernia Mountain
Serro Drago
SA 62
AP 2
D'Orgaro Mountain
Samo
Africo
La Verde River
Casalnuovo
SA 12
38° 02' 30"
16° 00' 55"
2000 m
LEGEND PROFILE
Holocenic cover
Stilo Capo d'Orlando Formation
Aspromonte Peloritani Unit Terrains
Principal Normal Faults
Samo Africo Window metamorphic rocks
Thrusts

Fig. 2a

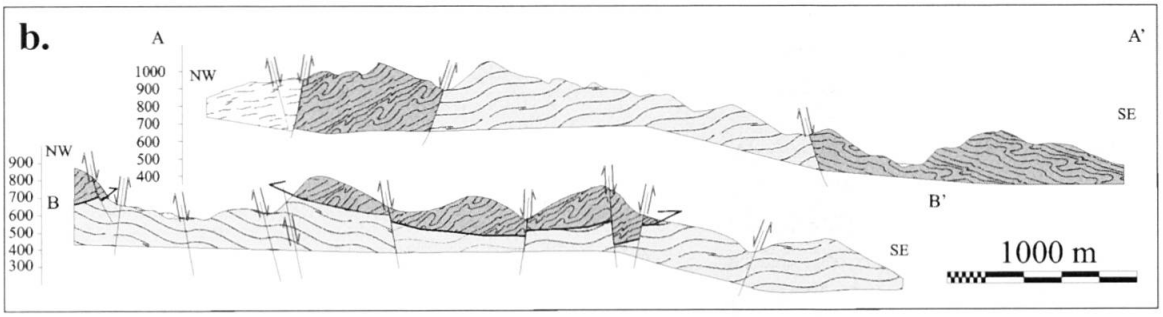

Fig. 2 (a) Geological map of study area. (b) Cross sections.

Polsi Unit), characterised by low- to medium-grade metapelites (Fig. 1b).

In the present study, the central-eastern tectonic window, partially corresponding to the Africo Unit of Messina et al. (1992), is called the Samo-Africo Complex (SAC). It is made up of a greenschist-facies metapelitic-metapsammitic sequence with minor layers of metacarbonates, characterised by early LT–HP metamorphism and a later lower-pressure mylonitic stage, also involving the lower portion of the overlying APU (Fig. 2). The high-grade metamorphic rocks of the APU extend across the Strait of Messina to the Peloritani Mountains and represent the uppermost unit of this nappe-edifice. It overlies a phyllitic Paleozoic unit, known as Mandanici Unit, and over a terrigenous-carbonatic Mesozoic–Cenozoic fragmentary cover, called the Alì sequence (Cirrincione and Pezzino, 1991, 1994). The Mandanici Unit and Alì sequence show an Alpine subgreenschist to greenschist-facies metamorphic overprint that developed at about 26 Ma (Atzori et al., 1994).

The tectono-stratigraphic sequence of the CPO southern sector terminates with the widely distributed conglomerates and turbiditic sandstones of the Late Oligocene–Early Burdigalian Stilo-Capo d'Orlando Formation (SCOF) (Bonardi et al., 1980b; Cavazza, 1988; Cavazza et al., 1997). This formation is topped (Fig. 1b) by a clay-rich mélange (Varicolori Clays) attributed to back-thrusting (Ogniben, 1960) or re-sedimentation (Cavazza et al., 1997).

3. Tectonometamorphic evolution

According to most authors, the dominant metamorphism in the southern sector of the CPO basement rocks is generally due to the Variscan orogeny. However, in the southern Aspromonte Massif, only sporadic fragments of the SU metapelites are characterised exclusively by a Hercynian fabric, whereas the main structures found in the APU and SAC are generally related to pervasive Alpine mylonitic deformation of Late Oligocene age (Bonardi et al., 1987; Pezzino et al., 1990, 1992; Platt and Compagnoni, 1990). Pre-mylonitic relics found in the APU are related to retrograde Hercynian HT–LP metamorphism whereas, in the SAC pre-mylonitic relics are ascribed to early LT–HP Alpine metamorphism.

Abbreviations used in the text are: D_n^{APU} and D_n^{SAC}: n^{-th} deformation phases in APU and in SAC, respectively; M_n^{APU} and M_n^{SAC}: crystallisation events, where index n indicates the relative chronology of the event. Where the index is not specified (e.g., $D_n - D_{n+1}$), the deformation phase occurs in both units.

3.1. Pre-mylonitic deformation phases and metamorphism

The rocks of the Aspromonte-Peloritani Unit are essentially characterised by strong Alpine mylonitic foliation, which becomes pervasive near the tectonic contact with the underlying basement rocks of the Samo-Africo Complex. Nevertheless, relics of early isoclinal folding, related to the first Variscan deformational phase (D_1^{APU}), are found aligned along the mylonitic foliation. According to Bonardi et al. (1987), the D_1^{APU} folding event belongs to the Variscan orogeny, peaking by 330 Ma, which produced the oldest identifiable metamorphic surface (S_1^{APU}) (Fig. 3a). [1]

Under the microscope, the metapelites of the APU show a syn-kinematic assemblage of $Qtz+Pl_1+Bt_1+Wm_1+Grt_1\pm Kfs_1\pm Sil$ defining the

[1] The subscripts of S (foliation), L (lineation) and B (plunge of fold axis) derive from the relative deformational event (e.g. S_2^{APU} from D_2^{APU}). Mineral abbreviations after Kretz (1983); additional abbreviations are: Wm, white mica (solid solution of Ms, Pg and Phn); Kfs, K-feldspar, and Amph, generic amphibole.

S_1^{APU} surface (Figs. 4a–5a), replaced by widespread coarse-grained recrystallisation of Wm_2, which developed during late-stage rehydration of the Kfs_1+Sil assemblage. Locally, late porphyroblasts of And_1 also occur. During the D_1^{APU} event, amphibolites and amphibole-bearing gneiss developed a $Qtz+Pl_1+Bt_1+Hbl_1\pm Grt_1$ assemblage, with local retrograde flakes containing oligoclase (Pl_2) and actinolite ($Amph_2$).

The microcrenulation of S_1^{APU} represents the subsequent deformation phase (D_2^{APU}), locally producing a S_2^{APU} schistosity, given by the aligned growth of $Qtz+Pl_3+Wm_3\pm Bt_2\pm Grt_2\pm Chl_1\pm And_2$ (Figs. 3a, 4a, 5b).

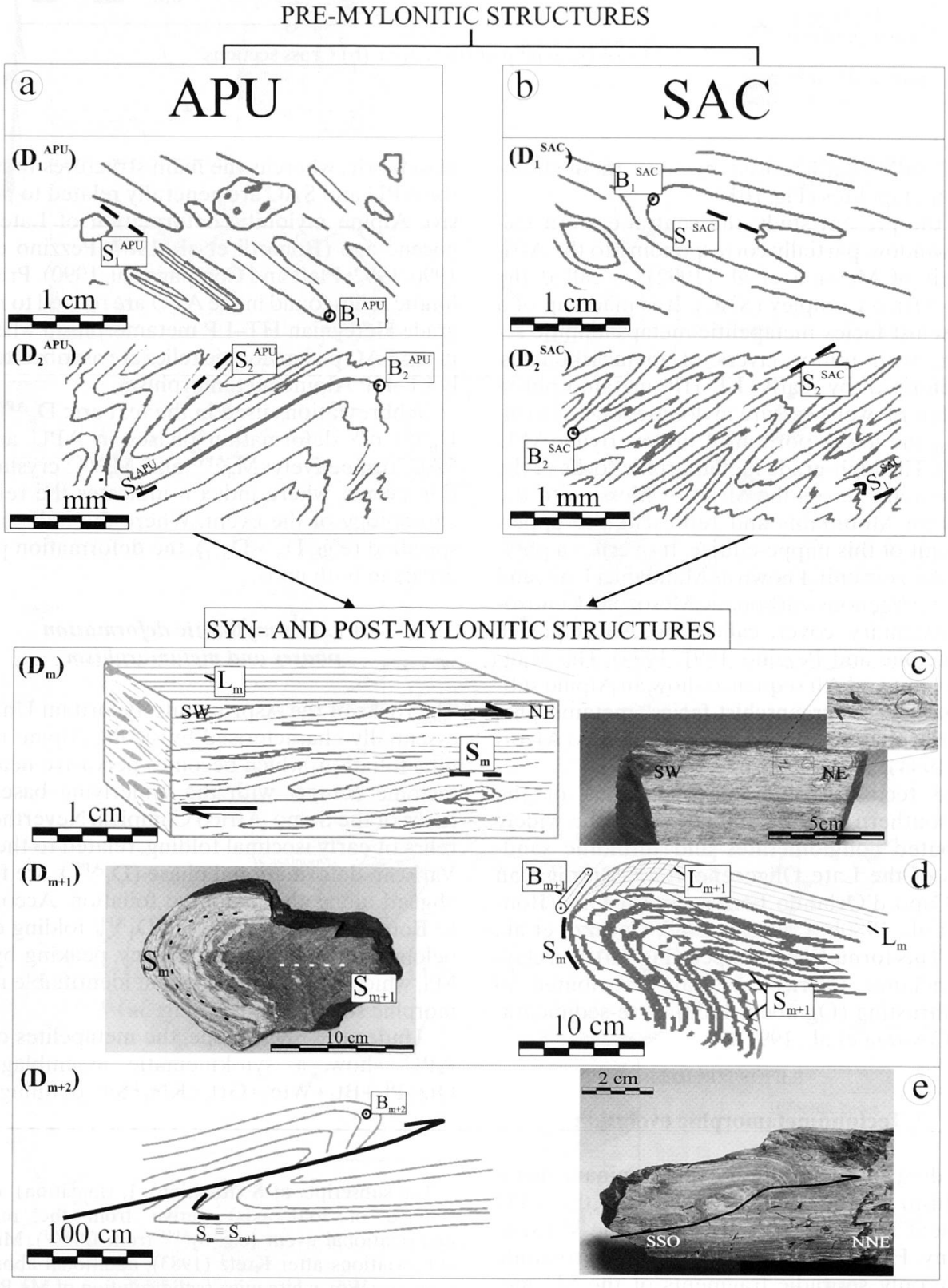

Fig. 3 Tectono-metamorphic evolution of Aspromonte-Peloritani Unit and Samo-Africo Complex.

The oldest deformation phase identified in the SAC (D_1^{SAC}) is represented by isoclinal folds, producing an axial planar foliation S_1^{SAC}, defined in the southern sector by low-grade mineral assemblages ($Qtz+Pl_1+Chl_1+Wm_1+Ep_1\pm Grt_1\pm Rt$) and evolving in the northern sector into higher-grade assemblages ($Qtz+Pl_1+Grt_1+Wm_1+Ep_1\pm Amph_1\pm Chl_1\pm Rt\pm Ttn\pm Ilm$) (Figs. 3b, 4b, 5c).

This evolution suggests the existence, within the SAC, of an early relic metamorphic field gradient, with grade increasing toward the north, which is interpreted as LT–HP metamorphism related to crustal thickening, as recognised in the ophiolitic units of northern Calabria (Schenk, 1980; Van Dijk et al., 2000; Rossetti et al., 2001).

A local crenulation cleavage (S_2^{SAC}) indicates the second deformation phase (D_2^{SAC}), locally leading to the crystallisation of $Qtz+Pl_2+Chl_2+Wm_2$ (Figs. 3b, 4b, 5d).

3.2. Syn- and post-mylonitic deformation phases and metamorphism

The subsequent deformation phase (D_m) developed during the Late Oligocene–Early Miocene overthrust of the APU upon the SAC, along a deep-seated compressional shear zone. In the rocks of both units, the effect of the consequent mylonitisation produces both a pervasive mylonitic foliation (S_m) and a pervasive stretching lineation (L_m). Locally, D_m totally replaces the pre-existing foliations and produces a great reduction in grain size, especially in the leucocratic gneiss of the APU (Fig. 3c).

The attitudes of the S_m foliation have an average strike direction of N45, with dips of 20°–80° to the SE or NW (Fig. 6). The stretching lineation (L_m) is oriented approximately SW–NE, plunging 15–35° alternatively SW or NE in both units (Fig. 6). In the present-day geographic coordinates, several types of kinematic indicators show a top-to-NE direction of shear in both units (Figs. 3c–7).

These structural data are consistent with Oligocene–Miocene Africa-verging orogenic transport, in view of the fact that the Aspromonte Massif was affected by major counter-clockwise rotation (60–70°) during the Late Oligocene–Recent south-east migration of the CPO (Scheepers, 1994; Scheepers et al., 1994; Rosenbaum and Lister, 2004). During this time, retrograde green-

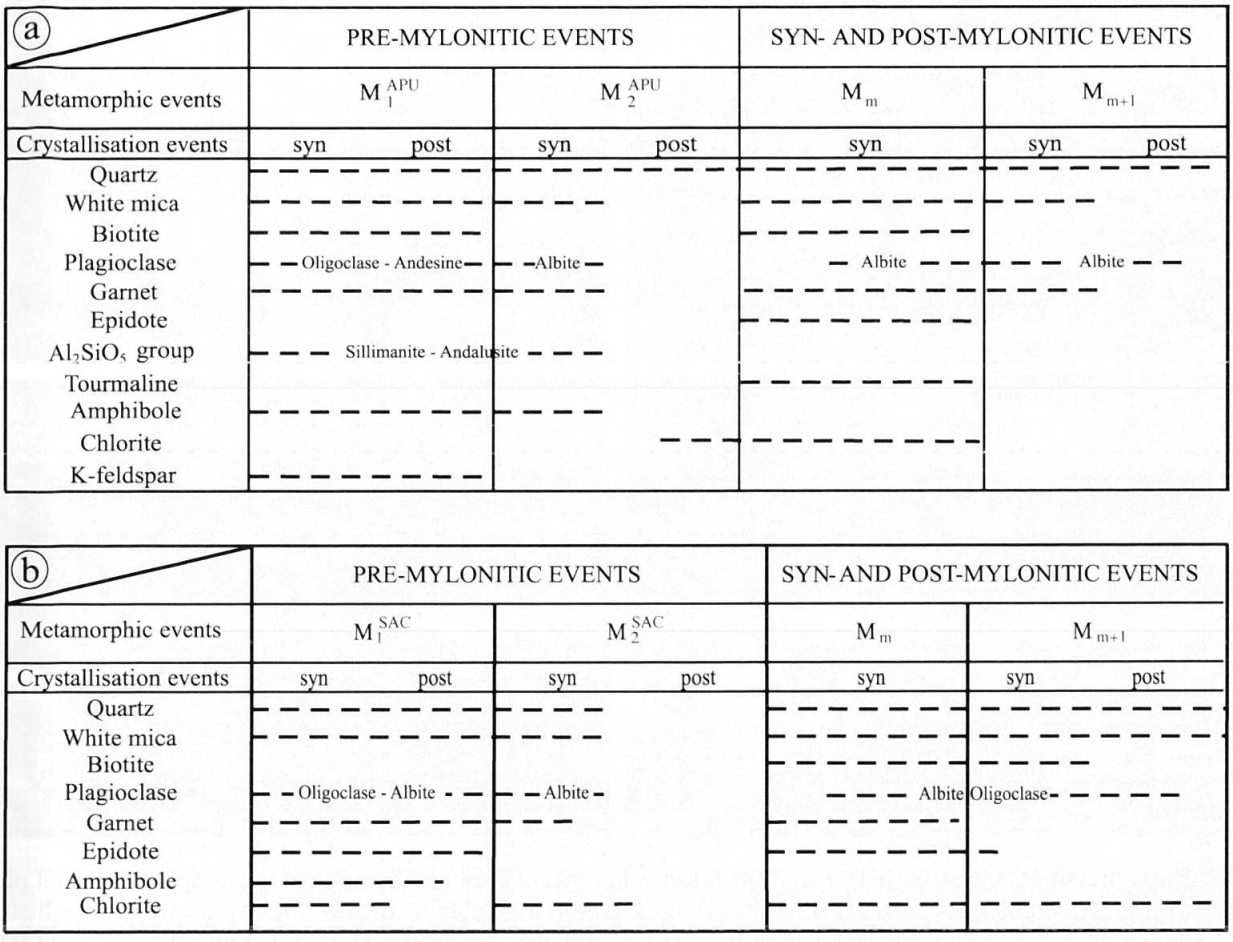

Fig. 4 Relationship between deformation phases and crystallisation events: (a) in Aspromonte-Peloritani Unit; (b) in Samo-Africo Complex.

schist-facies metamorphism developed along the S_m foliation, defined by syn-kinematic growth of $Qtz+Bt_3+Wm_3+Chl_1+Ep_1\pm Grt_3\pm Pl_3\pm Tur_1$ and $Qtz+Wm_4+Chl_3+Ep_2\pm Bt_1\pm Grt_3\pm Pl_3$ in the APU and SAC, respectively (Figs. 4–7).

The effect of the mylonitic event on the deformation behaviour of the single mineral phase varies due to different intracrystalline deformation mechanisms operating during strain evolution. More particularly, in the southern-sector lithotypes of both units, brittle-plastic deformation behaviour of mineral phases may be observed, with microfractured sigmoidal garnet aggregate and bookshelf-sliding feldspars producing antithetic fractures with respect to the direction of shear; these two phases are surrounded by granoxenoblastic ribbon-like quartz (Fig. 7 c,d,d',e,f,f'). In this area, ribbon-like quartz shows a dominant dislocation glide deformation mechanism with limited grain boundary migration, especially on basal glide planes in the (c)<a> direction. This is demonstrated by the asymmetric cross-girdle quartz c-axis fabric, obtained by an image-assisted analysis computer program on thin sections cut perpendicular to the mylonitic foliation and parallel to the stretching lineation (Fig. 8 c,d,e,f) (StereoNett 2.0; Duyster, 1996).[2]

In the northern sector of the study area, the D_m deformation phase frequently involved high-temperature deformation mechanisms, testified

[2] The crystallographic orientation of the quartz c-axis was computed with AVA diagrams (AVA= Achsenverteilungsanalyse; Sander, 1950) using StereoNett 2.0 software (Duyster, 1996). This software applies image-analysis techniques to calculate the azimuth and inclination of quartz c-axes for every position within the field of view by recording the changing birefringence colours while the microscope stage is rotated by 90° (AAVA method - Automatische AchsenVerteilungs Analyse). A detailed description of the procedure is given in Appendix A of Stöckhert and Duyster, (1999) and on web site http://www.microtexture.de/StereoHTML/quarzava.htm.

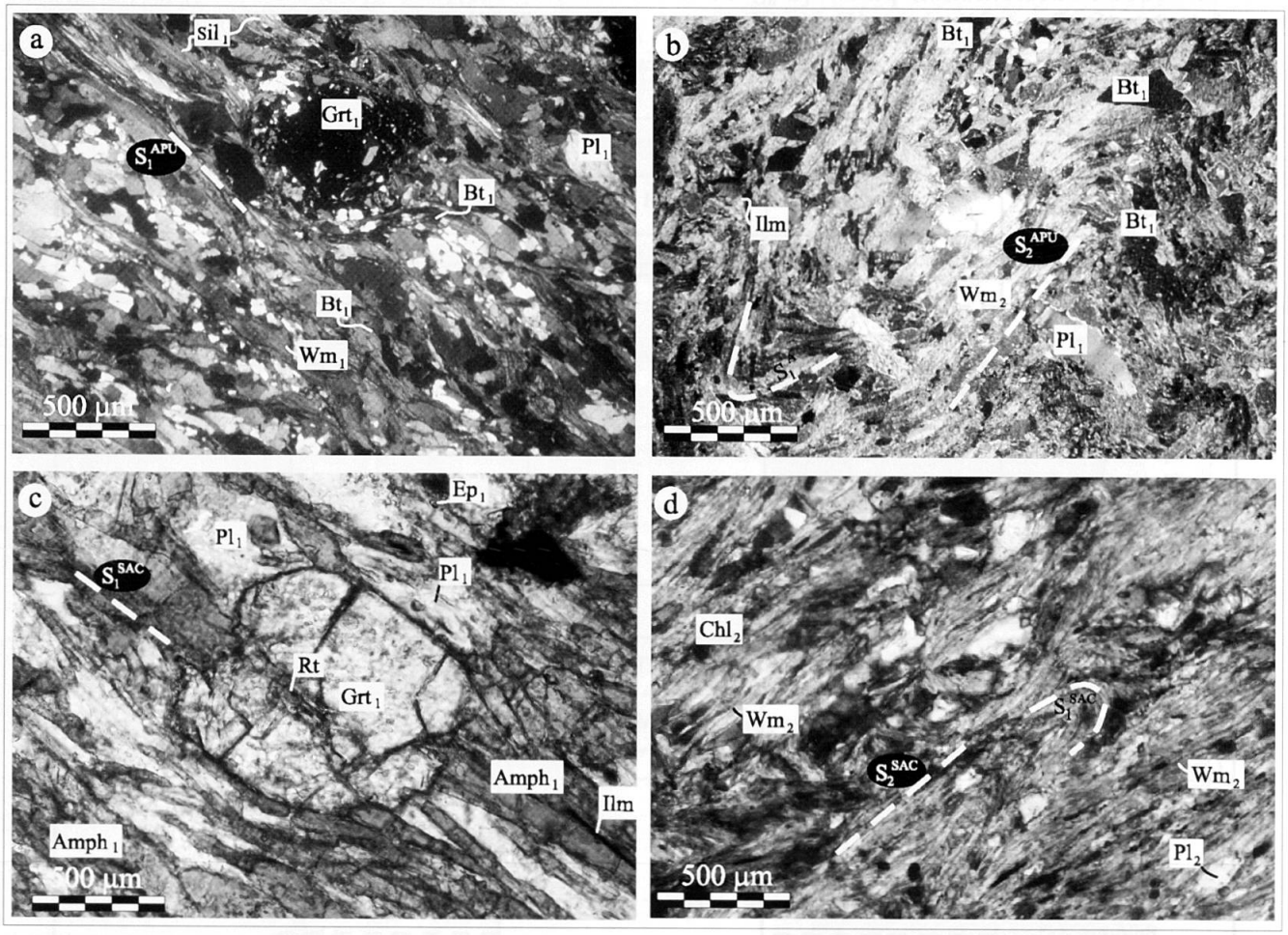

Fig. 5 Early metamorphic assemblages in Aspromonte-Peloritani Unit and Samo-Africo Complex: (a) axial planar schistosity (S_1^{APU}) highlighted by $Qtz+Pl_1+Bt_1+Wm_1+Grt_1+Sil$ assemblage (nicols +); (b) crenulation schistosity (S_2^{APU}) developing in lepidoblastic levels (nicols +); (c) axial planar schistosity (S_1^{SAC}) in amphibole-bearing schists of northern SAC, highlighted by $Qtz+Grt_1+Pl_1+Amph_1+Ilm+Rt$ assemblage (nicols +); (d) micro-crenulation of S_1^{SAC} foliation with development of S_2^{SAC} crenulation schistosity and crystallisation of $Qtz+Pl_2+Chl_2+Wm_2$ (nicols +).

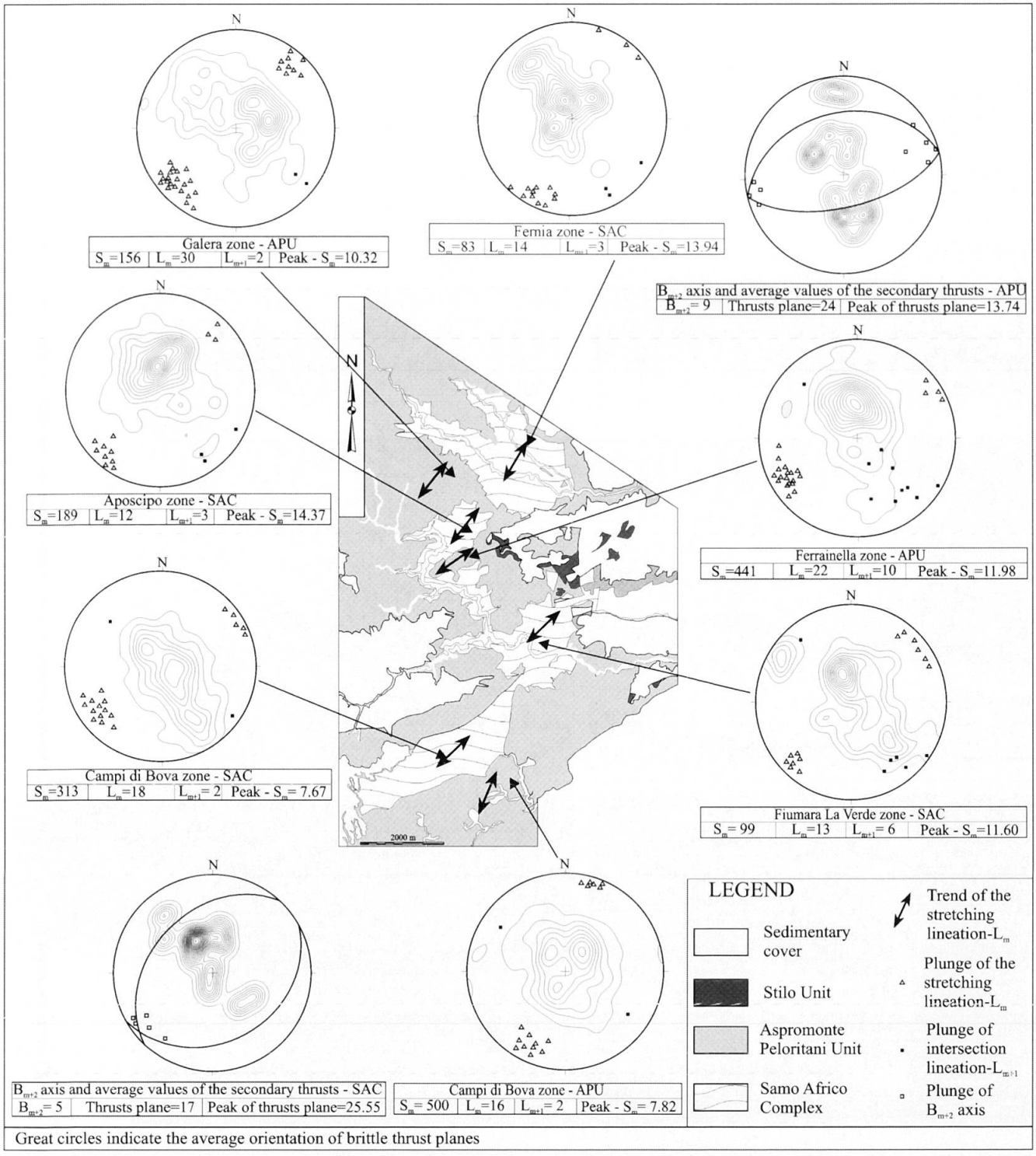

Fig. 6 Map of study area: Stereoplot (lower hemisphere) of attitude of mylonitic foliation (S_m), plunge of stretching lineation L_m, B_{m+1} fold axes, intersection lineation L_{m+1}, orientation of brittle thrust plane, and plunge of B_{m+2} axis (see text for explanation).

by both syn-kinematic growth of biotite and feldspar affected by synthetic bookshelf-sliding structure, surrounded by totally recrystallised ribbon-like quartz (Fig. 7a–b). These fabrics indicate a combined sub-grain rotation and grain boundary migration recrystallisation regime, as demonstrated by both oblique foliation (Passchier and Trouw, 1996) (Fig. 7 b') and progressive activation of the prism {m}<c> slip system toward the north. The top-to-the-NE and/or NNE direction of shear is also confirmed by the quartz c-axis orientation pattern (Fig. 8 a,b,c,d).

The subsequent deformation phase (D_{m+1}) produced in both units isoclinal folds of the mylonitic foliation (S_m) from macroscopic to microscopic scales (Figs. 3d–9), producing a local axial planar foliation (S_{m+1}), which becomes pervasive only in the leucocratic gneiss of the APU. This

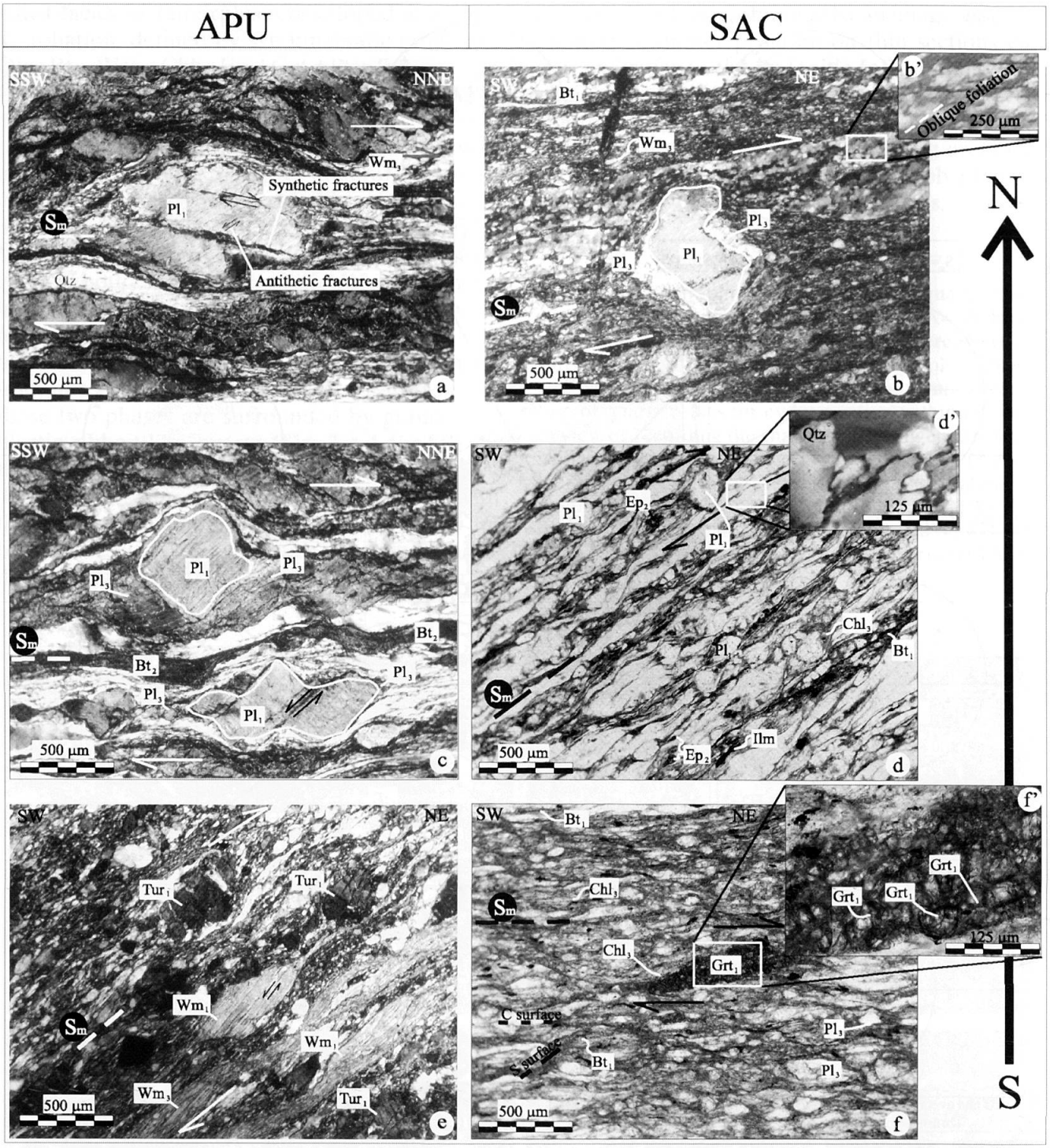

Fig. 7 Syn-mylonitic (D_m event) metamorphic microstructures and assemblages in Aspromonte-Peloritani Unit (left column) and Samo-Africo Complex (right column) from south to north. (a) Synthetic and antithetic fractures in feldspar porphyroclast (nicols crossed); (b) σ-type plagioclase porphyroclast (nicols crossed), with: b') oblique foliation in recrystallised ribbon-like quartz (nicols crossed, with gypsum plate); (c) δ-type and antithetic microfaults in plagioclase porphyroclasts (nicols crossed); (d) ribbon-like quartz levels (nicols parallel), with: d') *grain boundary migration* phenomena (nicols crossed); (e) mica-fish and syn- to post-mylonitic crystal growth of tourmaline (nicols crossed); (f) sigmoidal garnet aggregate (nicols parallel), with: f') brittle effects in microcrystalline garnets (nicols parallel).

folding event affected the lithotypes of both units and also the mylonitic thrust contact, with consequent transposition of the latter and the development of irregular layering with repetition, at different scales, of the rocks of the two units. This event represents the space-time evolution of the compressional shear zone during exhumation of the crystalline basement rocks.

The macroscopic fold axes (B_{m+1}) show SE–NW orientations, plunging 5–15° SE or NW, coin-

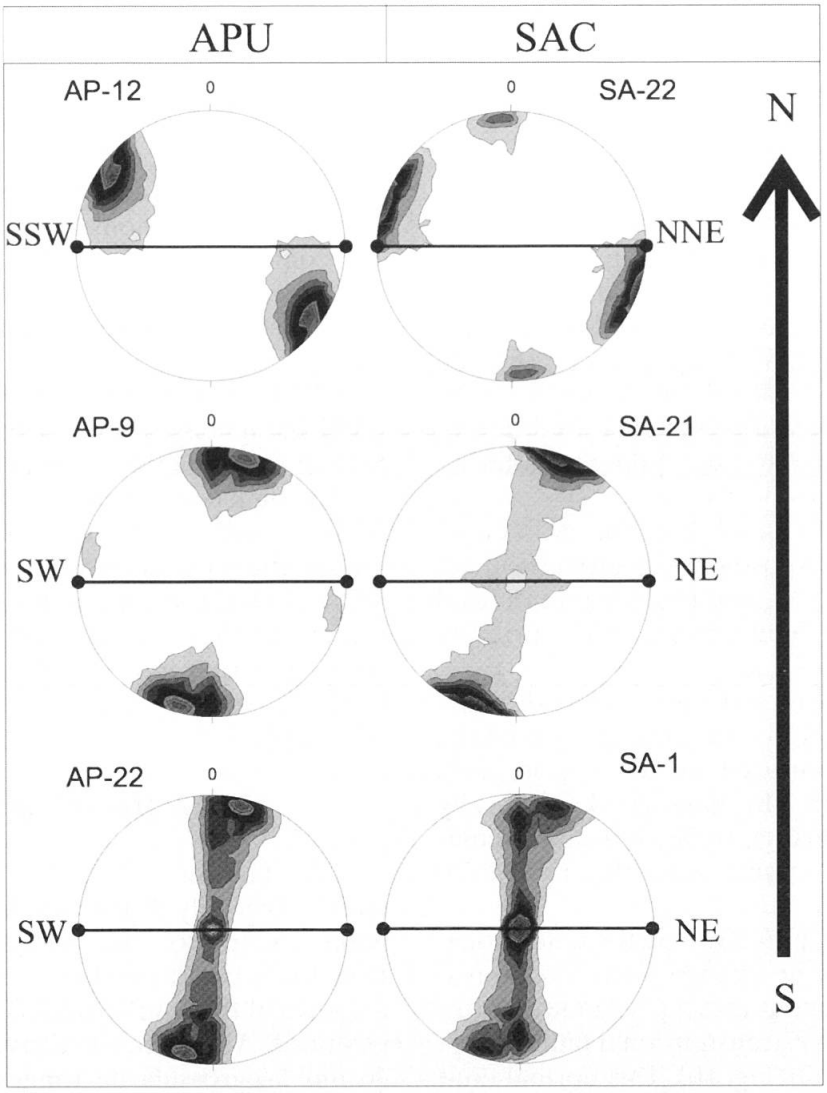

Fig. 8 Quartz c-axis orientation pattern of APU (left column) and SAC (right column) mylonitic rocks from southern to northern sector of study area (see text for explanation).

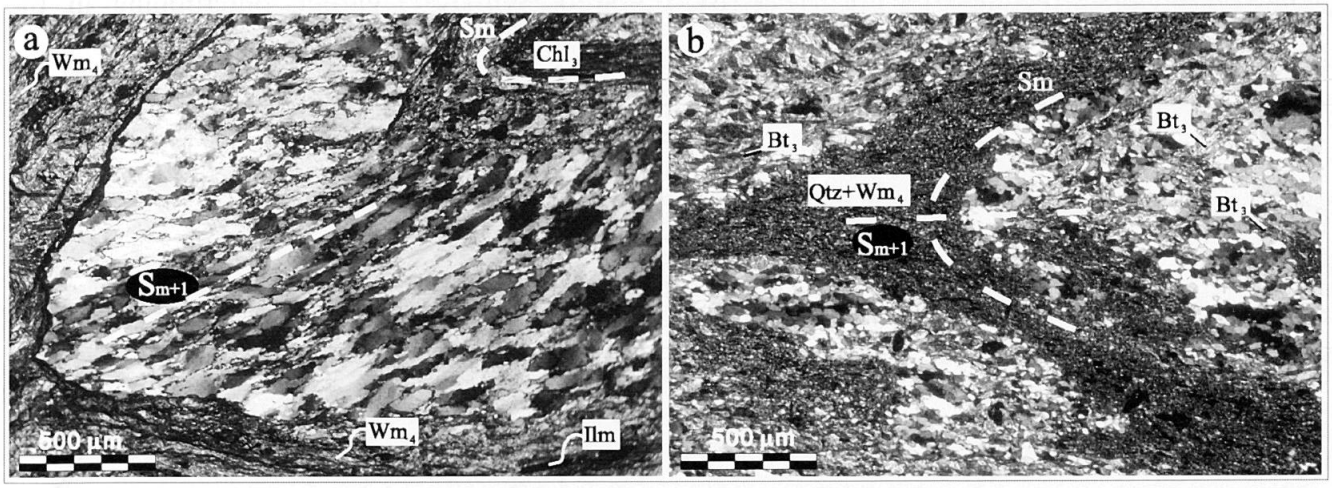

Fig. 9 Syn-D_{m+1} metamorphic assemblages in Aspromonte-Peloritani Unit and Samo-Africo Complex: (a) Qtz+Wm_4+Pl_4 assemblage of APU (nicols crossed); (b) Qtz+Pl_4+Wm_4+Bt_3 assemblage of SAC (nicols crossed).

ciding with the related intersection lineation (L_{m+1}) represented by rods, drag folds and microfolds (Figs. 3d–6).

During the D_{m+1} event in the APU rocks, growth of white mica (Wm_5) and overgrowths of garnet (Grt_4) rims and new plagioclase (Pl_4) are

observed (Fig. 9a). In the SAC, the syn-S_{m+1} assemblage $Qtz+Pl_4+Wm_4+Bt_2+Ep_3+Chl_4$ occurs, especially in the northern sector (Fig. 9b).

3.3. Late and brittle deformation phases

The evolution of the compressional thrust belt proceeded at shallower conditions, producing SE-verging metric to hectometric asymmetrical folds (D_{m+2}) (Fig. 3e) with average axis orientations from WSW–ENE to SW–NE (B_{m+2} in Fig. 6). The thrust-sheet system evolved, producing a conjugate secondary brittle thrust system on a different scale, oriented N45–N65 and plunging alternatively SE or NW (Figs. 3e–6).

This thrust system remobilised the earlier ductile shear zone, transposing the tectonic contact between APU and SAC and causing pronounced thickening of the mylonitic band, which currently ranges from 0.5 to 0.8 km.

This last compressional shear event thrusted the SU onto the underlying APU along a brittle shear zone, partly sutured by the syn-orogenic deposition of SCOF. The base of SCOF locally shows secondary thrusts, which indicate a compressional tectonic regime persisting until mid-Miocene time.

Subsequently a NE–SW brittle extensional fault system marks the change from a compressional to an extensional tectonic regime, accommodated by a NW–SE transtensional fault system (e.g., Buonamico fault; Fig. 1b). This normal fault system was also responsible for the longitudinal uplift of the Aspromonte Massif and of the transversal basin structures, which cross the Aspromonte Massif horst structure to the north (Fig. 1b).

4. Rock and Mineral Composition

Fourteen representative samples of SAC and five of APU were selected for study of the bulk rock and mineral compositions. Sample locations are shown in Fig. 2. Analytical conditions and representative compositions of bulk analyses and mineral composition are listed in Appendix 1.

4.1. Bulk composition

The SAC garnet-muscovite-bearing schists and APU paragneisses are essentially homogeneous in their major element contents.

The bulk composition of the metapelitic rocks of both units confirms protoliths of pelitic to semipelitic type, as shown in the $Fe_2O_3^{tot}/K_2O$ vs. SiO_2/Al_2O_3 classification diagram (Fig. 10a), indicating that these sedimentary protoliths originated at an active continental margin, as suggested by the K_2O/Na_2O vs. SiO_2 discrimination diagram (Fig. 10b).

4.2. Mineral chemistry

4.2.1. Garnet

Garnet is widely distributed in all of the analysed rocks, except for the lowest-grade metapelites from the SAC. Pre-mylonitic sigmoidal garnet aggregates of the southern SAC show uniform compositions. Almandine is consistently higher than 46 mol%, grossularite ranges from 24 (average core composition) to 19 mol% (average rim composition), and spessartine from 10 (core) to 17 mol% (rim). Subordinate pyrope (4–6%) is observed. Syn-D_1^{SAC} garnet, outcropping in the

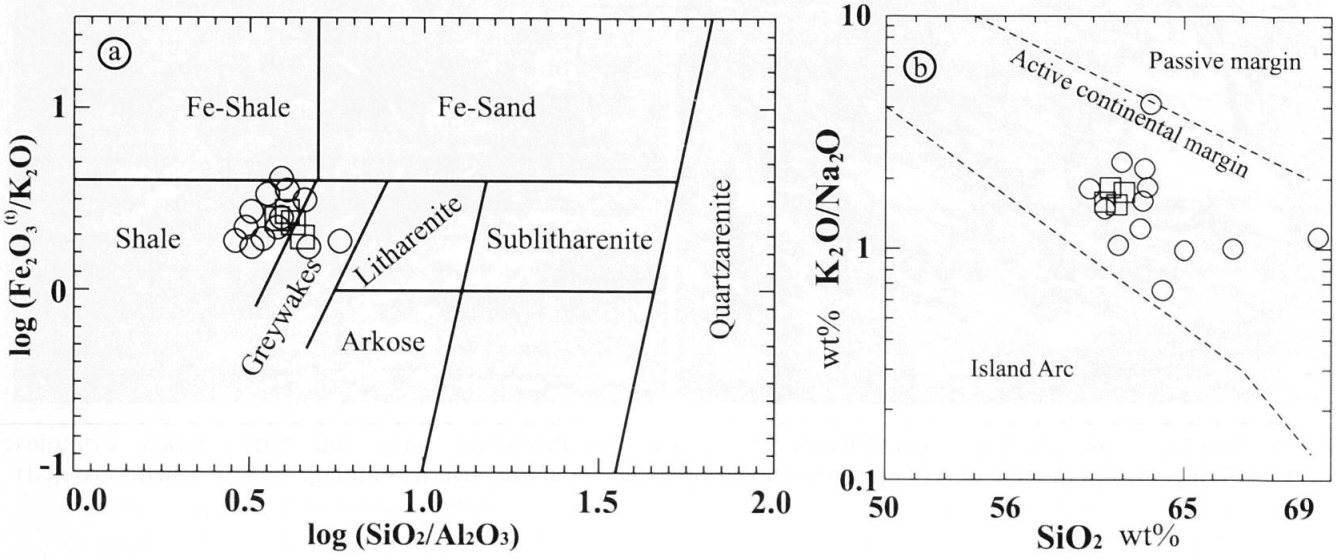

Fig. 10 (a) Discrimination diagram log (SiO_2/Al_2O_3) *vs.* log ($Fe_2O_3^{(t)}/K_2O$) from Herron (1988) showing shale composition of studied metapelites; (b) Discrimination diagram wt% SiO_2 *vs.* wt% K_2O/Na_2O, after Roser and Korsch (1986) to indicate geotectonic setting. Squares APU – Circles SAC.

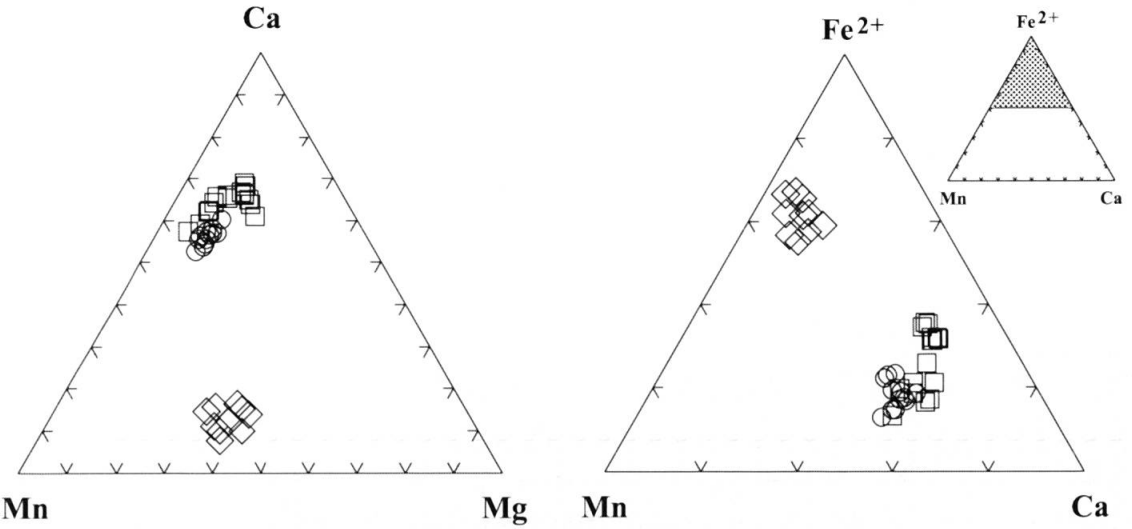

Fig. 11 Compositional variation of garnet from APU and SAC . Squares and circles: syn-D_1^{SAC} garnets of northern and southern SAC. Diamonds: syn-D_1^{APU} garnets of APU.

northern SAC, shows slightly higher grossularite (29 mol% in the core) compared with those of the southern SAC (Fig. 11)[3].

Syn-D_1^{APU} garnet is very different from the pre-mylonitic garnet of the SAC. In the APU, almandine is similar or slightly higher (65–70 mol%) than in the SAC, while grossularite is lower (4–7 mol%); pyrope (9–12 mol%) and spessartine (16–20 mol%) are higher (Fig. 11).

[3] Average values of garnet composition of SAC were obtained on 30 and 19 point analyses for core and rim compositions, respectively.

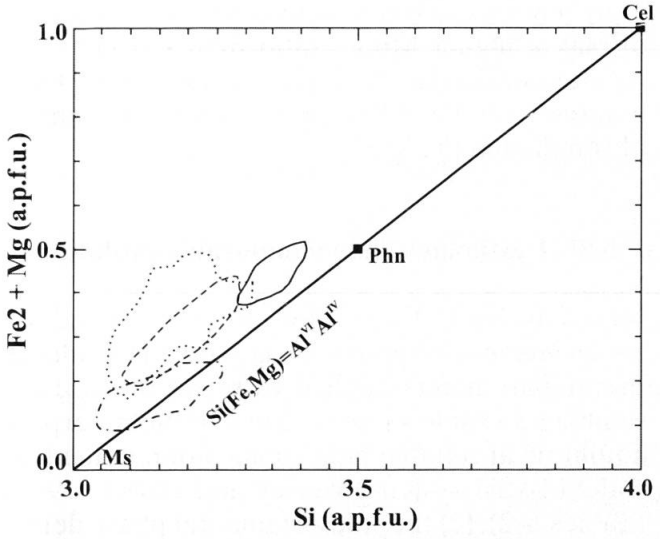

Fig. 12 Compositional variations of white mica in APU and SAC. Continuous and dotted lines: pre- and syn-mylonitic white mica of SAC. Dashed-dotted and dashed lines: pre- and syn-mylonitic white mica of APU.

4.2.2. Biotite

Biotite in SAC metapelites is rare, except in the amphibole-bearing schists of the northern sector, where it is locally more abundant than white mica. It grew exclusively during the D_m and D_{m+1} events and shows uniform composition compared with the syn-D_m and/or syn-D_{m+1} found in the APU (X_{Fe} about 0.5; Al^{IV} content ranging between 2.1–2.7 a.p.f.u; Ti content between 0.03–0.22 a.p.f.u). By contrast, syn-D_1^{APU} biotite is different in composition and is classified as Fe-biotite, with higher Al^{IV} content (2.8 a.p.f.u).

4.2.3. White Mica

Syn-D_1^{SAC} white mica reveals significant phengite content and a relatively homogeneous composition (Si ranging between 3.35 and 3.44 a.p.f.u). It shows higher Fe–Mg and lower paragonite (Na/(Na+K) = 0.1–0.2) than the late syn-D_m and syn-D_{m+1} white mica of the same unit (Fig. 12).

Syn-D_1^{APU} white mica has low phengite (Si = 3.0–3.1 a.p.f.u), whereas the composition of the syn-mylonitic white mica has intermediate phengite contents, comparable with the syn-D_m white mica of the SAC (Fig. 12).

4.2.4. Plagioclase

Syn-D_1^{SAC} plagioclase contains between 9 and 18 mol% anorthite, suggesting relic LT pre-mylonitic assemblages for the rocks belonging to the SAC (Fig. 13).

In APU paragneiss, pre-mylonitic zoned plagioclase has anorthite contents ranging from 30–50 mol% (core) to 5–10 mol% (rim), suggesting a higher metamorphic grade for the pre-mylonitic protolith of this unit than in the SAC.

Pre-kinematic K-feldspar is abundant in the

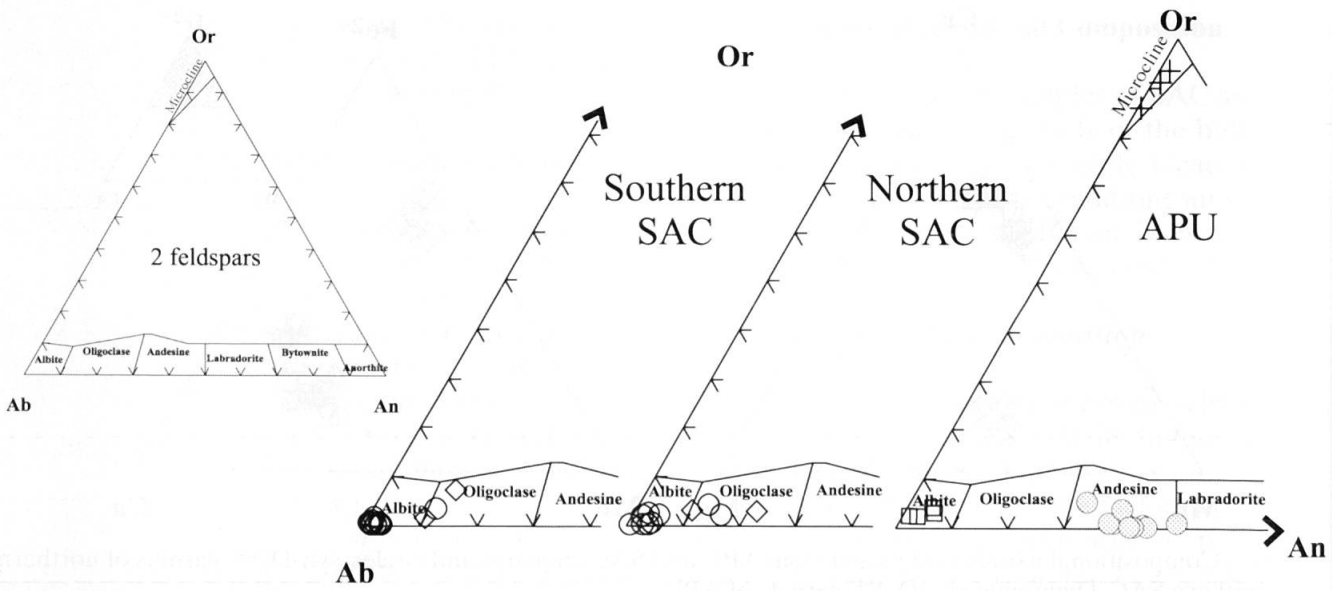

Fig. 13 Compositional variations of feldspars in APU and SAC. Diamonds and empty circles: pre- and syn-mylonitic plagioclases of SAC. Grey circles and squares: pre- and syn-mylonitic plagioclases of APU. Crosses: K-feldspars of sample AP-20 (laminated leucocratic gneiss of APU).

leucocratic gneiss of the APU and is characterised by a decrease in K/Na, ranging from 94.6 mol% orthoclase (core) to 80.1 mol% (rim) (Fig. 13).

Syn- to post-mylonitic plagioclase of both units is characterised by anorthite contents <4 mol%, except for some retrograde oligoclase rims bounding syn-D_m albite in the SAC. This last evidence indicates overgrowth during the decompressional path of the SAC (Fig. 13).

4.2.5. Amphibole

Syn-D_1^{SAC} amphibole shows compositions ranging from tschermakite hornblende to barrosite hornblende, with relatively high contents of Na_{M4} (0.625–2.0 a.p.f.u), low Ti (0.035 a.p.f.u) and Al (1.90–2.7 a.p.f.u).

In the APU rocks, amphibole is classified as Mg-hornblende, with retrograde flakes of tschermakite to actinolite composition. They have relatively low Na_{M4} (0.120–0.241 a.p.f.u), while Al and Ti contents range from 1.67 to 3.1 a.p.f.u and from 0.009 to 0.145 a.p.f.u, respectively.

4.2.6. Chlorite

Chlorite is widespread in all rocks of the APU. It occurs only as a retrograde phase on biotite and amphibole. In the SAC rocks, it occurs along the C-plane of the mylonitic foliation (S_m); its composition ranges from ripidolite to pychnochlorite.

4.2.7. Other Minerals

In the SAC rocks, epidote crystallised both during the first deformational phase (D_1^{SAC}) and D_m and D_{m+1} phases. The first generation has relatively high values of Fe^{3+} ($X_{pistacite}$ = 0.22–0.26) and may be classified as Al-epidote. The second generation has lower pistacite component ($X_{pistacite}$ = 0.14), consistent with a clinozoisitic composition. The APU syn-D_m epidotes show similar composition to those crystallising during the same deformational event in the SAC.

Tourmaline grew mainly during the D_m event and is quite common in the APU laminated leucocratic gneiss (Fig. 7e). It often shows inverse Fe–Mg zoning from core to rim. Rutile, related to the HP pre-mylonitic event, is found as inclusions in the syn-D_1^{SAC} garnet.

Ilmenite is the most common accessory mineral in the rocks of both units; syn-D_1^{APU} crystals display a higher Mn/Fe ratio than syn-D_1^{SAC} ilmenite, confirming the higher metamorphic temperature of the APU pre-mylonitic metamorphism than in the SAC.

5. P–T estimates and metamorphic evolution

Metamorphic P–T conditions were estimated using an integrated approach based on: (a) available thermobarometers applied to select mineral assemblages (Table 1); (b) calculated metamorphic equilibria at suitable bulk composition in the NaCaKFMASH system (Worley and Powell, 1998) (Tables 1–2); (c) the study of mineral phase deformation behaviour (Table 1).

The first approach was applied choosing assemblages characterised by a clearcut textural equilibrium.

Selected metamorphic equilibria were calculated using the PERPLEX software package, assuming SiO_2 and O_2 to be excess thermodynamic components and H_2O an excess phase component (Connolly, 1990) (Table 2). The internally consistent database and the compensated Redlich-Kwong fluid equation of state of Holland and Powell (1998 – updated by Connolly, 2005, pers. comm.)[4], were used in computations of thermodynamic equilibria.

The P–T range of the retrograde mylonitic event was also constrained by means of the quartz, feldspar and garnet deformation behaviour in mylonites of both units.

5.1. Pre-mylonitic metamorphism

The earliest identifiable assemblage in the APU rocks (M_1^{APU}) consists of quartz, andesine, almandine garnet (with low grossularite contents), sillimanite, biotite, muscovite s.s ± K-feldspar. This paragenesis is strongly overprinted by a retrograde assemblage, comprising static coarse-grained muscovite s.s. and syn-kinematically grown quartz, oligoclase, biotite, almandine garnet (with low grossularite content) and andalusite (M_2^{APU}) (Table 2).

According to the estimated mineral composition of equilibrium 1, calculated for AP-2 bulk-composition (Table 2), the M_1^{APU} assemblage is characterised by pressures ranging from 0.39 to 0.5 GPa and temperatures from 650° to 675 °C, as constrained by the intersection with the 3.1 Si-content curve (Massonne and Schreyer, 1987) (Tables 1–2; Fig. 14a). The resulting P–T values confirm HT–LP peak metamorphic conditions, ascribed to the Variscan evolution of the Aspromonte-Peloritani Unit.

The subsequent metamorphic event (M_2^{APU}) developed at lower P–T conditions (P 0.25–0.42 GPa; T 510°–560 °C), confirming the retrograde evolution of the Variscan metamorphism. This is

[4] See Appendix 2 for solid-solution model glossary.

Table 1 Average P-T estimates of Samo Africo Complex and Aspromonte Peloritani Unit samples.

Method and reference	Southern SAC	Northern SAC	APU
Peak temperature estimates			
Grt-Bt thermometry (*Ferry* and *Spear*, 1978)			**520° ± 30°C**
Grt-Bt thermometry (*Perchuk* and *Laurentva*, 1983)			**545° ± 30°C**
Grt-Bt thermometry (*Bhattacharya* et al., 1992)			**500° ± 30°C**
Grt-Phe thermometry (*Hynes* & *Forest*, 1988)	**470° ± 30°C**	**490° ± 30°C**	
Grt-Amph thermometry (*Graham* and *Powell* 1984)		**545° ± 25°C**	
Amph-Pl thermometry (*Holland* and *Blundy*, 1994)		**540° ± 20°C**	
Equilibrium 1			**675° ± 20°C**
Pressure at peak estimates			
GASP barometer (*Koziol*, 1989)			**0.2 – 0.3 GPa**
Al content in Amphibole (*Hammarstrom* and *Zen*, 1986)		**1.1 ± 0.1 GPa**	
Si content in phengite (*Massonne* and *Schreyer*, 1987)	**0.95 – 1.05 GPa**	**0.95 – 1.2 GPa**	**0.390 – 0.45 GPa**
Equilibrium 1			**0.275 – 0.725 GPa**
Retrograde temperature estimate			
Deformation behaviour of mineral phases (*Hirt* and *Tullis*, 1992; *Pryer*, 1993; *Passchier* and *Trouw*, 1996)	**460° – 320°C**	**500° – 320°C**	**500° – 350°C**
Equilibrium 2			**550° ± 10°C**
Equilibrium 3			**450° ± 20 °C**
Equilibrium 4	**520° ± 10°C**		
Equilibrium 5	**450° ± 15°C**		
Equilibrium 6		**530° ± 20°C**	
Equilibrium 7		**410° ± 20°C**	
Retrograde pressure estimate			
Equilibrium 2			**0.425 ± 0.2 GPa**
Equilibrium 3			**0.6 ± 0.25 GPa**
Equilibrium 4	**0.6 ± 0.025 GPa**		
Equilibrium 5	**0.45 ± 0.15 GPa**		
Equilibrium 6		**0.575 ± 0.01 GPa**	
Equilibrium 7		**0.4 ± 0.15 GPa**	
Si content in phengite (*Massonne* and *Schreyer*, 1987)	**0.25 – 0.65 GPa**	**0.25 – 0.65 GPa**	**0.39 – 0.75 GPa**

Equilibria are calculated by PERPLEX (*Connolly* and *Petrini*, 2002)

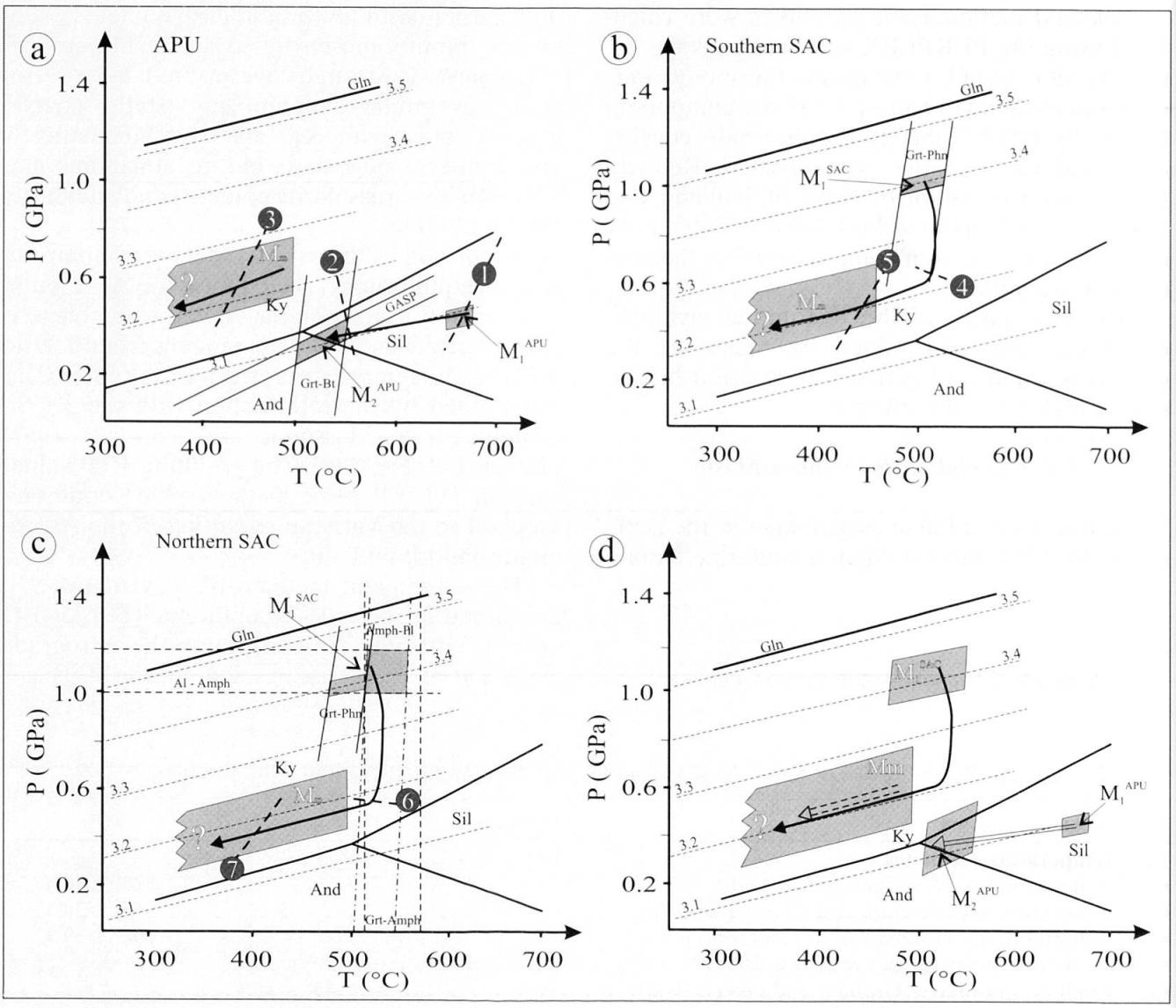

Fig. 14 Estimated P–T path of APU and SAC: (a) P–T evolution of APU constrained by use of: equilibria 1 and 2 representing syn-M_1^{APU} and syn-M_2^{APU} assemblages calculated for sample bulk composition (AP-2) (see text for explanation); Grt–Bt thermometry (Ferry and Spear, 1978; Perchuk and Lavrent'eva, 1983; Bhattacharya et al., 1992); GASP barometer of Koziol (1989); grey area: P–T values of syn-mylonitic event derived from behaviour of mineral phases during shear event, confined by isopleths of Si content (Massone and Schreyer, 1987) (see text for explanation); equilibrium 3: retrograde mineral assemblage developing during mylonitic event calculated for sample bulk composition (AP-2) (see text for explanation); (b) – (c) P–T evolution of southern and northern SAC, constrained by use of: Grt–Phe thermometer of Hynes and Forest (1988); dashed-dotted lines: Amph–Pl thermometer of Holland and Blundy (1994); vertical dashed lines: Grt–Amph thermometer of Graham and Powell (1984); horizontal dashed lines: Al in Amph barometer of Hammarstrom and Zen (1986); grey area: P–T values of syn-mylonitic event derived from behaviour of mineral phases during shear event confined by isopleths of Si content (Massone and Schreyer, 1987) (see text for explanation). Equilibria 4 and 6: breakdown of pre-mylonitic grossularite-rich garnet for bulk composition of samples SA-12 and SA-62. Equilibria 5 and 7: retrograde mineral assemblages developing during mylonitic event for bulk composition of samples SA-12 and SA-62 (see text for explanation). (d) Schematic PT evolution of APU and SAC. Single continuous arrow: entire PT evolution of SAC; double continuous arrow: Variscan PT evolution of APU; double dashed arrow: mylonitic Alpine evolution of APU. Gln: glaucophane stability boundary (Carman and Gilbert, 1983). Al_2SiO_5 triple point is from Holdaway (1971).

constrained both by equilibrium 2 and by the intersection between the garnet-biotite thermometer (Ferry and Spear, 1978; Perchuk and Lavrent'eva, 1983; Bhattacharya et al., 1992) and GASP barometer (Koziol, 1989)(Tables 1–2; Fig. 14a).

In the SAC metapelites, the earliest identifiable metamorphic assemblage (M_1^{SAC}) consists of quartz, almandine garnet (with high grossularite content), white mica (with relatively high phengite content), oligoclase and epidote (Table 2).

The M_1^{SAC} thermometric estimates, ranging

Table 2 Bulk composition of selected samples. Composition of mineral assemblages in different metamorphic events. Calculated mineral assemblages in the NaCaKFMASH system.

Bulk composition in NaCaKFMASH system			
Location	APU	Southern SAC	Northern SAC
Selected samples	AP-2	SA-12	SA-62
Lithotypes	Garnet-Sillimanite Paragneiss	Garnet-Muscovite Schist	Garnet-Muscovite Schist
SiO_2	61.08	64.99	61.01
Al_2O_3	14.95	14.31	15.59
FeO^{tot}	7.62	6.74	9.23
MgO	5.14	2.97	4.38
CaO	3.31	1.36	1.31
Na_2O	1.86	2.49	1.61
K_2O	2.94	2.44	2.38
H_2O	excess	excess	excess
O_2	excess	excess	excess
Metamorphic event	Measured mineral compositions and recalculated end-members percentage for different metamorphic event		
M_1^{APU}	$Qtz+Pl(ab_{55}an_{45})+Bt(ann_{24}phl_{16}east_{24}sidph_{36})+Wm(mu_{90}cel_2fcel_8)+Chl(*)+Grt(alm_{79}gr_8py_{13})+Sil$	------	------
M_2^{APU}	$Qtz+Pl(ab_{70}an_{30})+Bt(ann_{30}phl_{30}east_{20}sidph_{20})+Chl(*)+Grt(alm_{78}\ gr_8py_{14})+And$	------	------
M_1^{SAC}	------	$Qtz+Pl(ab_{80}an_{20})+Wm(mu_{60}cel_{30}fcel_{10})+Chl(*)+Ep(cz_{60}fep_{40})+Grt(alm_{62}gr_{30}py_8)+Rt$	$Qtz+Pl(ab_{80}an_{20})+Grt(alm_{62}gr_{30}py_8)+Wm(mu_{55}cel_{35}fcel_{15})+Ep(cz_{60}fep_{40})+Rt$
M_2^{SAC}	------	$Qtz+Pl(ab_{95}an_5)+Chl(*)+Wm(mu_{80}cel_{10}fcel_{10})$	$Qtz+Pl(ab_{95}an_5)+Chl(*)+Wm(mu_{80}cel_{10}fcel_{10})$
M_m+M_{m+1}	$Qtz+Bt(ann_{32}phl_{28}east_{24}sidph_{16})+Wm(mu_{70}cel_{20}fcel_{10})+Ab+Chl(clin_{40}daph_{40}ames_{20})+Ep(cz_{75}fep_{25})$	$Qtz+Wm(mu_{80}cel_{10}fcel_{10})+Chl(clin_{45}daph_{35}ames_{20})+Ep(cz_{80}fep_{20})+Bt(ann_{25}phl_{25}east_{25}sidph_{25})+Pl(ab_{80}an_{20})$	$Qtz+Wm(mu_{80}cel_{10}fcel_{10})+Chl(clin_{42}daph_{33}ames_{25})+Ep(cz_{80}fep_{20})+Bt(ann_{25}phl_{25}east_{25}sidph_{25})+Pl(ab_{80}an_{20})$
Metamorphic evolution	Calculated mineral assemblages composition for NaCaKFMASH system		
HT Variscan evolution	1 $Pl(ab_{60}an_{20}or_{20})+Sil+H_2O\leftrightarrow Pl(ab_{60}an_{40})+Wm(mu_{100})+Qtz$	------	------
Retrograde Variscan evolution	2 $Pl(ab_{80}an_{20})+Grt(alm_{75}gr_{12.5}py_{12.5})+Wm(mu_{100})+H_2O\leftrightarrow Grt(alm_{88}gr_{12})+Pl(ab_{60}an_{40})+Bt(ann_{25}phl_{25}east_{25}sidph_{25})+Chl(clin_5daph_{45}ames_{50})+Qtz$	------	------
Breakdown reactions of Early Alpine garnet	------	4 $Bt(ann_{50}phl_{50})+PL(ab_{78}an_{22})+Wm(mu_{80}fcel_{20})+Grt(alm_{75}gr_{25})+H_2O\leftrightarrow Bt(ann_{50}sidph_{50})+Chl(clin_{50}daph_{50})+Pl(ab_{77}an_{23})+Qtz$	6 $Bt(ann_{50}phl_{50})+PL(ab_{70}an_{30})+Wm(mu_{80}fcel_{20})+Grt(alm_{75}gr_{25})+H_2O\leftrightarrow Bt(ann_{50}siphl_{50})+Chl(clin_{50}daph_{50})+Pl(ab_{68}an_{32})+Qtz$
Syn-mylonitic Late Alpine reactions	3 $Chl(daph_{100})+Bt(ann_{50}phl_{50})+Pl(ab_{80}an_{20})+Qtz+H_2O\leftrightarrow Ab+Chl(clin_{50}daph_{50})+Ep(cz_{80}fep_{20})+Wm(mu_{80}fcel_{20})+Qtz$	5 $Bt(ann_{50}phl_{50})+Chl(daph_{100})+Pl(ab_{82}an_{18})+Qtz+H_2O\leftrightarrow Chl(clin_{50}daph_{50})+Wm(mu_{80}fcel_{20})+Ep(cz_{80}fep_{20})+Ab+Qtz$	7 $Bt(ann_{50}phl_{50})+Chl(daph_{100})+Pl(ab_{80}an_{20})+Qtz+H_2O\leftrightarrow Chl(clin_{50}daph_{50})+Wm(mu_{80}fcel_{20})+Ep(cz_{80}fep_{20})+Ab+Qtz$

* Data not available. End member abbreviations after Holland and Powell (1998). Number of reactions in the lower part of the table refers to equilibria number of Fig. 14.

between 480° and 520 °C, were evaluated using the garnet–phengite couple (Hynes and Forest, 1988) for estimated minimum pressures of 0.98–1.05 GPa obtained through the phengite content in white mica (Massonne and Schreyer, 1987) (Table 1; Fig. 14b–c).

For amphibole-bearing schists (northern SAC) the intersection between the garnet-amphibole (Graham and Powell, 1984), the amphibole-plagioclase (Holland and Blundy, 1994) geothermometers, and the geobarometer based on Al contents in amphibole (Hammarstrom and Zen, 1986) was applied. These yield higher M_1^{SAC} metamorphic peak condition than the metapelites of the same unit (P 1.0–1.2 GPa; T 520°–560 °C) (Table 1; Fig. 14c).

These discrepancies notwithstanding, the above estimates indicate for the M_1^{SAC} phase a relatively high-pressure metamorphism, which differs significantly from the early low-pressure

metamorphism (M_1^{APU}) of the APU. We interpret the M_1^{SAC} event as due to Early Alpine metamorphism related to crustal thickening, which developed upon subduction of the Mesozoic pelitic cover.

5.2. Syn- to post-mylonitic metamorphism

The metapelitic rocks of the APU and SAC contain a similar syn-mylonitic assemblage, consisting of quartz, albite, low phengite, Al-epidote, ilmenite, chlorite (ripidolite-pychnochlorite in composition) and biotite, with an average ratio of Fe/(Fe+Mg) = 0.52, differing only with the presence in the SAC of oligoclase reaction rims, which surround earlier albite porphyroblasts.

The bulk compositions of samples AP-2, SA-12 and SA-62 (simplified for the NaCaKFMASH system) (Table 2) were used to estimate equilibrium conditions pertaining to the retrograde metamorphic evolution.

During the D_m deformational event, the $Qtz+Wm_4+Chl_2+Pl_3+Ep_1$ assemblage developed at the expense of the $Qtz+Bt_1+Pl_1+Chl_1$ assemblage in APU metapelites; according to equilibrium 3 (Table 2), this reflects higher P (0.8–0.38 GPa) and lower T values (480°–410 °C) than the Variscan evolution (Tables 1–2; Fig. 14a).

The syn-D_m assemblage of the southern and northern SAC may be explained by the same retrograde evolution, which occurred in two phases.

The first phase involves breakdown of grossularite-rich garnet at lower P and at near-isothermal conditions (P 0.625–0.58 GPa; T 520 ± 30 °C), according to equilibria 4 and 6 (Tables 1–2; Fig. 14b–c). The resulting adiabatic decompression path of the SAC is also constrained by the presence of the oligoclase reaction rim surrounding earlier albite porphyroblasts.

The second phase is characterised by syn-kinematic growth of $Qtz+Wm_3+Chl_3+Ep_2+Pl_3\pm Bt_1$ in a P–T range of P 0.625–0.35 GPa; T 480°–380 °C, according to equilibria 5 and 6 (Tables 1–2; Fig. 14b–c).

For all the previous syn-shear T estimates (500°–380 °C), a minimum Pressure condition ranging from 0.625 to 0.35 GPa was constrained by Massonne and Schreyer's (1987) geobarometer (Si contents 3.15–3.28) for both units (Table 1; Fig. 14a–b–c).

The deformation behaviour of mineral phases confirms that the mylonites developed between upper and lower greenschist-facies conditions. In particular, syn-mylonitic ribbon-like quartz of the southern sector of the study area is characterised by a dominant dislocation glide deformation mechanism with limited grain boundary migration. In the northern sector, this evolved into a combined sub-grain rotation and grain boundary migration recrystallisation regime (Fig. 7a–b). The progressive changes in the quartz slip-system regime, from an asymmetric cross-girdle c-axis orientation pattern (south) to an orientation pattern with the c-axis lying subparallel (15°–30°) to the stretching lineation (north) (Fig. 8), indicates a north-verging increase in temperature from 400 °C to 600 °C in a hydrous regime (Hirth and Tullis, 1992; Passchier and Trouw, 1996).

The highest temperatures obtained appear to be an overestimate, in view of the fact that all of the mylonitic lithotypes (in the southern and northern sector) are characterised by brittle deformation behaviour of feldspar and garnet (Fig. 7c,d,e,f). Syn-mylonitic growth of biotite and the activation of synthetic fractures in bookshelf-sliding feldspar are observed in the northern sector (Fig. 7a–b), confirming higher shearing temperatures toward the north. In this context a reliable upper T limit of the shear phase consistent with all observations is >420 °C (Pryer, 1993), but <500 °C (Passchier and Trouw, 1996).

The present P–T path indicates Late Alpine shearing at conditions evolving from upper to lower greenschist-facies, associated with rapid adiabatic uplift of a deep-seated shear zone linked to nappe emplacement, which occurred during the compressional shear stage of the Africa-verging collisional event.

6. Discussion and conclusions

The multidisciplinary approach adopted in the present paper allowed us to unravel the tectonometamorphic evolution of the Aspromonte-Peloritani Unit and Samo-Africo Complex, offering a new geodynamic scenario for the southern sector of the Calabrian Peloritani Orogen.

The mylonitic event, which thrust the Aspromonte-Peloritani Unit onto the Samo-Africo Complex along a thick mylonitic band, marks the beginning of the joint structural and metamorphic history of these two units. Before this event, the two units had undergone very different tectonometamorphic evolutions.

According to most authors (Bonardi et al., 1987; Pezzino et al., 1990, 1992; Platt and Compagnoni, 1990; Messina et al., 1992, 1996), the earlier tectonometamorphic evolution of the APU was characterised by Hercynian retrograde polyphase evolution, represented by relic layering (S_1^{APU}) given by the syn-M_1^{APU} assemblage, locally crenulated (S_2^{APU}) and partially overprinted by the syn-M_2^{APU} assemblage (Table 2).

The peak P–T conditions (0.39–0.5 GPa; 650°–675 °C) are consistent with LP amphibolite-facies metamorphism (Fig. 14d). By contrast, the earlier tectonometamorphic evolution of the SAC was characterised by low- to medium-temperature peak metamorphic conditions, consistent with pre-mylonitic relic metamorphism emphasised by the syn-M_1^{SAC} assemblage (Table 2), locally crenulated (S_2^{SAC}) and partially retrogressed in the M_2^{SAC} assemblage (Table 2). Measured peak P–T conditions (0.98–1.2 GPa; 480°–560 °C) indicate a lower (southern SAC) to upper (northern SAC) greenschist-facies metamorphism, developed under HP conditions (Fig. 14d).

This information indicates that the peak P–T conditions of the SAC pertain to early crustal thickening, probably during the (Late Cretaceous?) Europe-verging subduction of thinned continental crust from the Adria margin beneath the European continental block. This stage is geochronologically related to the LT–HP ophiolitic units of northern Calabria, clearly representative of the HP Alpine metamorphism in the CPO (Schenk, 1980; Van Dijk et al., 2000; Rossetti et al., 2001).

In this new tectonic reconstruction, the SAC represents the natural southern continuation of the micaschists and amphibole-schists of the Madonna dei Polsi Unit (Pezzino et al., 1990, 1992; Puglisi and Pezzino, 1994), rather than the lower greenschist-facies metapelites belonging to the Variscan Africo Unit of Messina et al. (1992).

The syn-mylonitic assemblages found in rocks belonging to both units have close compositional affinity, suggesting this joint tectonometamorphic history, which evolved from 500° to 350 °C, with P ranging from 0.775 to 0.325 GPa (Fig. 14d). These conditions, according to Pezzino et al. (1990) and Puglisi and Pezzino (1994), refer to an Alpine shearing event of Late Oligocene age (Bonardi et al., 1987), which developed during uplift and exhumation of the crystalline basement rocks along a deep-seated compressional shear zone, rather than by horizontal extensional exhumation as invoked by Platt and Compagnoni (1990).

In both units, the shearing phase in the southern sector gave rise to a pervasive stretching lineation (L_m), usually oriented SW–NE, passing north to SSW–NNE orientation (Fig. 6). Along the L_m lineation, identified non-coaxial kinematic indicators show a top-to-the-NE or NNE direction of shear in the present-day geographic coordinates (Figs. 7–8). In this context, major counterclockwise rotation (60°–70°) occurred in the Aspromonte Massif during the Oligocene–Recent south-east migration of the CPO (Scheepers, 1994; Rosenbaum and Lister, 2004), indicating original Africa-verging (ESE) orogenic transport.

The presence of preserved HP relic assemblages, oligoclase reaction rims and post-mylonitic isoclinal folds (D_{m+1}) indicate fast uplift of the SAC, compatible with syn-convergent exhumation of a relatively HP metamorphosed sedimentary sequence.

Emplacement of the compressional thrust-belt persisted until the Early Miocene, as shown by thin-skinned SE-verging thrust-sheet planes involving the base of the Stilo-Capo d'Orlando Formation. This shallow thrust-sheet system produced both a pronounced thickening of the mylonitic band (present-day thickness 0.5–0.8 km) and an overlap of the external crystalline basement unit (Stilo Unit) with the Aspromonte-Peloritani Unit, along a brittle thrust plane.

According to Gueguen et al. (1998), the change from a compressional to an extensional tectonic regime began to operate for the CPO during the Late Burdigalian, associated with the opening of the Valivov basin and consequent separation of the CPO from the Sardinia block. The latter event is recorded in the CPO northern sector by brittle features operating from Late Miocene times (Cello et al., 1996). Brittle extensional tectonics are represented in the southern sector of the CPO by a NE–SW normal fault system, accommodated by a NW–SE transtensional fault system shown, for example, by the Buonamico fault (Fig. 1b).

The identification, in the deeper crystalline basement rocks (SAC) of relic Early Alpine HP metamorphic rocks exhumed in compressional regimes, opens up a possible new alternative tectonic frame, partly contrasting with the extensional exhumation model of HP metamorphic rocks proposed by Platt and Compagnoni (1990). In this new frame, the occurrence of a suture zone with Alpine HP–LT metamorphism (SAC) may be interpreted as resulting from a complete orogenic cycle, including Europe-verging (Late Cretaceous?) subduction, followed by a Late Oligocene collisional phase responsible for rapid extrusion along an adiabatic decompression path. In this context, SAC P–T evolution implies exclusively Alpine metamorphism affecting the Mesozoic sedimentary sequence, as found in the anchimetamorphic Mesozoic–Cenozoic Alì sequence (Peloritani Mountains) (Cirrincione and Pezzino, 1991, 1994; Atzori et al., 1994) and in the Madonna di Polsi Unit (central and northern Aspromonte Massif) (Pezzino et al., 1990, 1992; Puglisi and Pezzino, 1994).

In this new tectonic frame, the two lowermost crystalline basement units outcropping in the Aspromonte area represent a portion of an active

continental margin, which, following subduction, was extruded along the suture of the collision zone.

This interpretation modifies the geological framework and consequent geodynamic scenario of earlier studies (Bonardi et al., 1987; Platt and Compagnoni, 1990; Messina et al., 1992, 1996). It needs to be corroborated by structural and petrological reviews of the entire Aspromonte area, complemented by new "in situ" geochronological data, to improve our understanding of the complex polymetamorphic and polyorogenic metamorphic evolution of the CPO southern sector.

Acknowledgements

The critical reading of Martin Engi and Giacomo Prosser gave useful and fundamental suggestions, improving greatly the paper. We are sincerely grateful to Daniele Castelli for his constructive support in the application of the thermobarometrical data. We are also grateful to Rosalda Punturo for her helpful suggestions. Gabriel Walton is acknowledged for her careful revision of the English version.

References

Alvarez, W. (1976): A former continuation of the Alps. *Geol. Soc. Am. Bull.* **87**, 891–896

Amodio Morelli, L., Bonardi, G., Colonna, V., Dietrich, D., Giunta, G., Ippolito, F., Liguori, V., Lorenzoni, S., Paglionico, A., Perrone, V., Piccarreta, G., Russo, M., Scandone, P., Zanettin-Lorenzoni, E. and Zuppetta, A. (1976): L'arco calabro-peloritano nell'orogene appenninico-maghrebide. *Mem. Soc. Geol. It.* **17**, 1–60.

Atzori, P., Cirrincione, R., Del Moro, A. and Pezzino, A. (1994): Structural, metamorphic and geochronologic features of the Alpine event in south-eastern sector of the Peloritani Mountains (Sicily). *Per. Mineral.* **63**, 113–125.

Bhattacharya, Mohanty L., Maji, A., Sen, S.K. and Raith, M. (1992): Non-ideal mixing in the phlogopite-annite binary: constraints from experimental data on Mg–Fe partitioning and a reformulation of the biotite–garnet geothermometer. *Contrib. Mineral. Petrol.* **111**, 87–93.

Bonardi, G., Messina, A., Perrone, V., Russo, M., Russo, S. and Zuppetta, A. (1980a): La finestra tettonica di Cardeto (Reggio Calabria). *Rend. Soc. Geol. It.* **3**, 3–4.

Bonardi, G., Giunta, G., Perrone, V., Russo, M., Zuppetta, A. and Ciampo, G. (1980b): Osservazioni sull' evoluzione dell'Arco Calabro-peloritano nel Miocene inferiore: la Formazione di Stilo-Capo d'Orlando. *Boll. Soc. Geol. It.* **99**, 365–393.

Tables in Appendix

Table A1 Bulk rock analyses of representative samples and relative mineral assemblages.

Location	Southern SAC			Northern SAC		APU	
Sample	SA-42	SA-11	SA-12	SA-62	SA-58	AP-2	AP-20
Lithotypes	Chlorite-Muscovite Schist	Garnet-Muscovite Schist	Garnet-Muscovite Schist	Garnet-Muscovite Schist	Amphibole-Muscovite Schist	Garnet-Sillimanite Paragneiss	Leucocratic Gneiss
SiO_2	71.79	63.89	64.99	61.01	55.85	61.08	73.13
TiO_2	0.68	0.76	1.09	0.77	1.45	0.85	0.08
Al_2O_3	12.50	15.74	14.31	15.59	12.92	14.95	15.51
Fe_2O_3	3.09	2.60	4.87	0.00	3.05	2.08	0.32
FeO	1.87	3.67	2.36	9.23	8.97	5.19	0.11
MnO	0.05	0.09	0.11	0.06	0.16	0.11	0.01
MgO	2.34	3.72	2.97	4.38	4.97	5.14	0.14
CaO	0.52	1.34	1.36	1.31	6.44	3.31	0.89
Na_2O	2.47	2.83	2.49	1.61	3.85	1.86	6.49
K_2O	2.75	1.87	2.44	2.38	0.19	2.94	2.38
P_2O_5	0.18	0.21	0.29	0.27	0.18	0.24	0.19
L.O.I.	1.55	2.88	2.47	2.87	0.97	1.69	0.75
TOT	99.80	99.60	99.74	99.98	99.01	99.43	99.99
Garnet		I	I	I	I	I	
Plagioclase	I, II	I, II	I, II	I, II	I	I, II	I, II
White mica	I, II	I, II	I, II	I, II	I	I, II	I, II
Biotite		II	II	II		I, II	
Epidote	I	I, II	I, II	I, II	I	II	
Amphibole					I		
Chlorite	II	II	II	II			II
Al_2SiO_5 polymorph						I	
K-feldspar							I

I and II indicate pre-mylonitic and syn- to post- mylonitic minerals, respectively.

Bonardi, G., Cello, G., Perrone, V., Tortorici, L., Turco, E. and Zuppetta, A. (1982): The evolution of the northern sector of Calabria-Peloritani Arc in a semiquantitative palinspastic restoration. *Boll. Soc. Geol. Ital.* **101**, 259–274.

Bonardi, G., Messina, A., Perrone, V., Russo, S. and Zuppetta, A. (1984): L'unita di Stilo nel settore meridionale dell'Arco Calabro-Peloritano. *Boll. Soc. Geol. It.* **103**, 279–309.

Bonardi, G., Compagnoni, R., Del Moro, A., Messina, A. and Perrone, V. (1987): Riequilibrazioni tettonico-metamorfiche Alpine dell'Unità dell'Aspromonte, Calabria Meridionale. *Rend. Soc. It. Min. Pet.* **42**, p. 301.

Borsi, S. and Dubois, R. (1968): Données geo-chronologiques sur l'histoire hercynienne et alpine de la Calabre centrale: C. R. Hebdomadaires Sci. Acad. Sci., Serie D: Sciences Naturelles **266**, 72–75.

Bouillin, J.P. (1984): Nouvelle interprétation de la liaison Apennin-Maghrébides en Calabre: conséquences

Table A2 Representative mineral analyses of garnet.

Rock	Metapelite						Amphibole-bearing schist	
Location	Southern SAC			Northern SAC	APU		Northern SAC	
Sample	SA-11(495)	SA-11 (494)	SA-12 (205)	SA-62 (381)	AP-2 (270)	AP-2(271)	SA-58 (250)	SA-58 (242)
Type	I	I	I	I	I	I	I	I
Zone	CORE	RIM	CORE	CORE	CORE	RIM	CORE	RIM
SiO_2	37.83	36.46	35.287	37.61	37.46	36.32	37.21	38.11
TiO_2	0.10	0.13	0.151	0.12	0.00	0.00	1.89	0.24
Al_2O_3	20.03	20.61	20.616	21.09	21.09	20.46	19.98	21.09
Cr_2O_3	0.02	0.00	0.082	0.03	0.03	0.01	0.02	0.04
FeO^{tot}	24.72	25.61	25.087	28.40	28.82	28.11	24.85	25.74
MnO	6.86	7.36	5.069	3.40	7.42	7.38	4.93	5.29
MgO	1.07	1.18	1.228	1.29	2.52	2.47	0.89	0.87
CaO	8.93	8.36	8.704	8.75	2.32	2.54	9.80	8.92
Na_2O	0.02	0.01	0.047	0.04	0.00	0.05	0.02	0.02
Total	99.56	99.71	96.271	100.71	99.64	97.34	99.58	100.31
Si	3.051	2.94	2.932	2.992	3.029	3.006	3.007	3.047
Al^{IV}	0	0.06	0.068	0.008	0	0	0	0
Sum_T	3.051	3	3	3	3.029	3.006	3.007	3.047
Al^{VI}	1.903	1.897	1.95	1.968	2.008	1.993	1.901	1.986
Fe_3	0	0.142	0.095	0.024	0	0	0	0
Ti	0.006	0.008	0.009	0.007	0	0	0.115	0.014
Cr	0.001	0	0.005	0.002	0.002	0	0.001	0.003
Sum_A	1.91	2.047	2.06	2.001	2.01	1.994	2.017	2.003
Fe_2	1.667	1.584	1.649	1.866	1.949	1.945	1.679	1.721
Mg	0.128	0.142	0.152	0.153	0.303	0.305	0.108	0.103
Mn	0.468	0.503	0.357	0.229	0.508	0.517	0.337	0.358
Ca	0.771	0.722	0.775	0.746	0.201	0.225	0.848	0.764
Na	0.003	0.001	0.008	0.006	0	0.008	0.003	0.002
Sum_B	3.039	2.953	2.94	2.999	2.961	3.001	2.976	2.95
Sum_cat	8	8	8	8	8	8	8	8
O	12	12	12	12	12	12	12	12
Alm	52.148	46.525	49.603	52.605	65.811	65.005	54.713	58.392
And	0	8.349	5.571	1.512	0	0	0	0
Gross	26.905	19.895	24.532	29.706	6.694	7.502	29.643	25.805
Pyrope	4.488	5.566	5.972	6.42	10.246	10.189	3.771	3.511
Spess	16.382	19.665	14.005	9.638	17.161	17.281	11.813	12.161
Uvaro	0.077	0	0.317	0.119	0.087	0.023	0.06	0.132

Location	Southern SAC		Northern SAC		APU	
Average-values	CORE	RIM	CORE	RIM	CORE	RIM
Alm	55.07	52.30	51.63	51.56	54.36	57.27
And	7.05	6.06	3.80	5.15	5.8	4.70
Gross	24.01	19.02	29.02	23.58	8.34	5.74
Pyrope	4.27	6.52	4.32	4.60	12.20	11.94
Spess	10.04	17.02	11.39	15.01	19.29	20.32
Uvaro	0.01	0.00	0.04	0.00	0.01	0.01

I: pre-mylonitic minerals. Average values of garnet composition of SAC metamorphic rocks obtained on 30 and 19 point analyses for core and rim composition, respectively and, for APU, on 21 and 12 point analyses for core and rim composition, respectively.

sur la paléogéographie téthysienne entre Gibraltar et les Alpes. *Rév. Géol. Dyn. Géogr. Phys.* **25**, 321–338.

Bouillin, J.P., Durand Delga, M. and Olivier, Ph. (1986): Betic-Rifian and Tyrrhenian Arcs: distinctive features, genesis and development stages. In: The Origin of Arcs (F. Wezel ed.) Elsevier, Amsterdam, 281–304.

Carman, J.H. and Gilbert, M.C. (1983): Experimental studies on glaucophane stability. *Am J. Sci.* **238 A**, 414–437.

Cavazza, W. (1988): La Formazione di Stilo-Capo d'Orlando: un possibile strumento per lo studio dell' evoluzione strutturale dell'Arco Calabro-Peloritano. *Rend. Soc. Geol. It.* **11**, 35–38.

Cavazza, W., Blenkinsop, J., Decelles, P.G., Patterson, R.T. and Reinhardt, E.G. (1997): Stratigrafia e sedimentologia della sequenza sedimentaria oligocenico-quaternaria del bacino calabro-ionico. *Boll. Soc. Geol. It.* **116**, 51–77.

Cello, G., Invernizzi, C. and Mazzoli, S. (1996): Structural signature of tectonic processes in the Calabrian Arc, southern Italy: evidence from the ocean-derived Diamante-Terranova unit. *Tectonics* **15**, 187–200.

Cirrincione, R. and Pezzino, A. (1991): Caratteri strutturali dell'evento Alpino nella Serie Mesozoica di Alì e nell'Unità metamorfica di Mandanici (Peloritani Orientali). *Mem. Soc. Geol. It.* **47**, 263–272.

Cirrincione, R. and Pezzino, A. (1994) Nuovi dati strutturali sulle successioni Mesozoiche metamorfiche dei Monti Peloritani orientali. *Boll. Soc. Geol. It.* **113**, 195–203.

Connolly, J.A.D. (1990): Multivariable phase diagrams: an algorithm based on generalized thermodynamics. *Am. J. Sci.* **290**, 666–718.

Connolly, J.A.D. (2005): "Pseudosection with PERPLE_X: A WWW Tutorial", Computer Library of the Institute of Mineralogy and Petrology, ETH-Zurich, Switzerland, (http://www.erw.ethz.ch/~jamie/perplex_pseudosection.html).

Connolly, J.A.D. and Petrini, K. (2002): An automated strategy for calculation of phase diagram sections retrieval of rock properties as a function of physical conditions. *J. Metam. Geol.* **20**, 697–708.

Crisci, G. M., Donati, G., Messina, A., Russo, S. and Perrone, V. (1982): L'Unità superiore dell'Aspromonte. Studio geologico e petrografica. *Rend. Soc It. Min. Petrol.* **38 (3)**, 989–1014.

Dercourt, J., Zonenshain, L.P., Ricou, L.E., Kazmin, V.G., Le Pichon, X., Knipper, A.L., Grandjacquet, C., Sorokhtin, O., Geyssant, J., Lepvrier, C., Sborshschikov, I.V., Boulin, J., Biju-Duval, B., Sibuet, J.C., Savostin, L.A., Westphal, M. and Laver, J.P. (1985): Présentation de 9 cartes paléogéographiques au 1/20.000.000 s'étendant de l'Atlantique au Pamir pour la période du Lias à l'Actuel. *Bull. Soc. Géol. France* **1**, 637–652.

Dewey, J.F., Helman, M.L., Turco, E., Hutton, D.H.W. and Knott, S.D., (1989): Kinematics of the western Mediterranean. In: M.P. Coward, D. Dietrich and

Table A3 Representative analyses of white-mica.

Rock	Metapelite								
Location	APU		Southern SAC				Northern SAC		
Sample	AP-2 (11)	AP-2 (12)	SA-12 (16)	SA-11 (499)	SA-12 (201)	SA-12 (206)	SA-62 (17)	SA-62 (374)	SA-62 (384)
Type	I	II	I	II	II	II	I	II	II
SiO_2	46.99	49.45	50.98	46.25	43.47	44.32	50.84	48.94	46.68
TiO_2	0.25	0.08	0.08	0.44	0.42	0.48	0.09	0.36	0.4
Al_2O_3	36.28	27.72	24.99	30.8	30.68	31.64	25.01	30.99	32.88
Cr_2O_3	0.05	0.02	0.04	0.04	0.05	0.05	0	0.01	0.03
FeO^{tot}	1.72	3.24	3.82	2.28	2.65	2.66	3.9	2.94	2.26
MnO	0	0.06	0.02	0.01	0	0	0.04	0.01	0.03
MgO	0.66	2.71	4.2	1.87	1.5	1.47	4.19	2.06	1.23
CaO	0	0.01	0.04	0.13	0.06	0.05	0.02	0	0.04
Na_2O	1	0.26	0.16	0.61	0.79	0.61	0.15	0.92	1.03
K_2O	7.96	10.34	10.76	10.09	9.63	9.15	10.6	10.43	10.32
Total	94.91	93.89	95.09	92.52	89.25	90.43	94.84	96.66	94.9
Si	3.095	3.364	3.443	3.189	3.119	3.12	3.441	3.237	3.14
Al^{IV}	0.905	0.636	0.557	0.811	0.881	0.88	0.559	0.763	0.86
Al^{VI}	1.909	1.584	1.431	1.69	1.711	1.743	1.435	1.651	1.745
Ti	0.012	0.004	0.004	0.023	0.023	0.025	0.005	0.018	0.02
Fe^{2+}	0.095	0.184	0.216	0.131	0.159	0.157	0.221	0.163	0.127
Cr	0.002	0.001	0.002	0.002	0.003	0.003	0	0.001	0.002
Mn	0	0.003	0.001	0.001	0	0	0.002	0.001	0.002
Mg	0.064	0.275	0.423	0.192	0.16	0.154	0.423	0.203	0.123
Ca	0	0.001	0.003	0.01	0.005	0.004	0.001	0	0.003
Na	0.128	0.034	0.021	0.082	0.11	0.083	0.02	0.118	0.134
K	0.669	0.898	0.928	0.888	0.882	0.822	0.915	0.88	0.886
Cations	6.879	6.984	7.029	7.019	7.053	6.991	7.022	7.035	7.042
O	11	11	11	11	11	11	11	11	11
Fe/FeMg	0.6	0.4	0.34	0.41	0.5	0.5	0.34	0.45	0.51
Mg/FeMg	0.4	0.6	0.66	0.59	0.5	0.5	0.66	0.55	0.49

I and II: pre-mylonitic and syn- to post- mylonitic minerals, respectively.

R.G. Park (Editors): Alpine Tectonics. *Geological Society London Special Publications* **45**, 265–283.
Duyster, J. (1996): Stereonett 2.0, University of Bochum http://www.microtexture.de/StereoHTML/quarzava.htm
Ferry, J.M. and Spear, F.S. (1978): Experimental calibration of the partitioning of Fe and Mg between biotite and garnet. *Contrib. Mineral. Petrol.* **66**, 113–117.
Fuhrman, M.L. Lindsley, D.H. (1988): Ternary feldspar modeling and thermometry. *Am. Mineral.* **73**, 201–215.
Ghisetti, F., Pezzino, A., Atzori, P. and Vezzani, L. (1991): Un approccio strutturale per la definizione della linea di Taormina: risultati preliminari. *Mem. Soc. Geol. It.* **47**, 273–289.
Graeßner, T. and Schenk, V. (1999): Low-pressure metamorphism of Palaeozoic pelites in the Aspromonte, southern Calabria: constraints for the thermal evolution in the Calabrian crustal cross-section during the Hercynian orogeny. *J. Metam. Geol.* **17(2)**, 157–172.
Graham, C.M., and Powell, R. (1984): A garnet-hornblende geothermometer: calibration, testing and application to the Pelona Schist, Southern California. *J. Metamorphic Geol.* **2**, 13–31.
Gueguen, E., Doglioni, C. and Fernandez, M. (1998): On the post-25 Ma geodynamic evolution of the western Mediterranean. *Tectonophysics* **298**, 259–269.
Hammarstrom, J.M. and Zen, E-An (1986): Aluminium in hornblende: an empirical igneous geobarometer. *Am. Mineral.* **71**, 1297–1313.
Herron, M.M. (1988): Geochemical classification of terrigenous sands and shales from core or log data. *J. Sedim. Petrol.* **58**, 820–829.
Hirth, G. and Tullis, J. (1992): Dislocation creep regimes in quartz aggregates. *J. Structural Geol.* **14**, 145–159.
Hynes, A. and Forest, R.C. (1988): Empirical garnet-muscovite geothermometry in low-grade metapelites, Selwyn Range (Canadian Rockies). *J. Metamorphic Geol.* **6**, 3, 297–309.
Holland, T.J.B. and Blundy, J. (1994): Non-ideal interactions in calcic amphiboles and their bearing on amphibole-plagioclase thermometry. *Contrib. Mineral. Petrol.* **116**, 433–447.
Holland, T.J.B., Baker, J. and Powell, R. (1998): Mixing properties and activity-composition relationships of chlorites in the system $MgO–FeO–Al_2O_3–SiO_2–H_2O$. *Eur. J. Mineral.* **10**, 395–406.
Holland, T.J.B. and Powell, R. (1998): An internally consistent thermodynamic data set for phases of petrological interest. *J. Metamorphic Geol.* **16**, 309–343.
Holdaway, J.R. (1971): Stability of andalusite and the alluminium silicate phase diagram. *Am. J. Sci.* **271**, 97–131.
Koziol, A.M. (1989): Recalibration of the garnet-plagioclase-Al_2SiO_5-quartz (GASP) geobarometer and

Table A4 Representative analyses of biotite and chlorite.

Rock	Metapelite						
Mineral	Biotite					Chlorite	
Location	APU		Southern SAC	Northern SAC			APU
Sample	AP-2 (287)	AP-2 (281)	SA-12 (194)	SA-62 (367)	SA-62 (371)	SA-12 (202)	AP-2 (285)
Type	I	II	II	II	II	II	II
SiO_2	33.57	36.00	35.68	39.54	33.45	25.50	24.66
TiO_2	2.13	1.62	1.78	0.24	0.18	0.08	0.08
Al_2O_3	19.69	19.38	16.73	28.93	25.62	22.87	22.69
Cr_2O_3	0.03	0.10	0.03	0.01	0.03	–	–
FeO^{tot}	21.44	15.61	17.96	12.34	19.96	24.16	22.32
MnO	0.15	0.13	0.16	0.05	0.13	–	–
MgO	8.52	10.10	9.47	7.06	10.47	16.28	16.68
CaO	0.00	0.09	0.26	0.06	0.06	0.03	0
Na_2O	0.13	0.12	0.13	0.43	0.47	0	0
K_2O	9.24	9.42	8.38	5.18	3.08	0.03	0
Total	94.90	92.57	90.57	93.83	93.43	88.98	86.43
Si	2.602	2.764	2.831	2.800	2.497	5.249	5.189
Al^{IV}	1.399	1.236	1.167	1.199	1.504	2.751	2.811
Al^{VI}	0.400	0.516	0.393	1.215	0.748	2.797	2.817
Ti	0.124	0.094	0.107	0.013	0.011	0.066	0.019
Fe^{2+}	1.389	1.003	1.191	0.731	1.246	4.158	3.928
Cr	0.002	0.006	0.002	0.001	0.002	–	–
Mn	0.010	0.008	0.011	0.003	0.008	–	–
Mg	0.984	1.157	1.120	0.746	1.165	4.991	5.231
Ca	0	0.008	0.022	0.005	0.005	0.007	–
Na	0.020	0.017	0.019	0.059	0.068	–	–
K	0.914	0.923	0.848	0.468	0.293	–	–
Cations	7.840	7.720	7.620	7.240	7.540	–	–
O	11	11	11	11	11	28	28
Fe/FeMg	0.59	0.46	0.52	0.5	0.52	0.45	0.43
Mg/FeMg	0.41	0.54	0.48	0.5	0.48	0.55	0.57

I and II: pre-mylonitic and syn- to post- mylonitic minerals, respectively.

application to natural paragenesis. EOS Trans. *Am. Geophys. Union* **70**, 493.
Kretz, R. (1983): Symbols for rock-forming minerals. *Am. Mineral.* **68**, 277–279.
Massonne, H.J. and Scheyer, W. (1987): Phengite geobarometry based on the limiting assemblage with K-feldspar, phlogopite and quartz. *Contr. Mineral. Petrol.* **96**, 212–224.
Messina, A., Compagnoni, R., De Francesco, A.M. and Russo, S. (1992): Alpine metamorphic overprint in the crystalline basement of the Aspromonte Unit (Calabrian-Peloritan Arc, Southern Italy). IGCP 276, *Newsletters* **5**, 353–379.
Messina, A., Russo, S. and Stagno, F. (1996): The Calabria-Peloritani Arc and its correlation with northern Africa and southern Europe. IGCP 276, **6**, 93–144.
Newton, R.C. and Haselton, H.T. (1981): Thermodynamics of the garnet-plagioclase-Al_2SiO_5-quartz geobarometer. In: Newton, R.C., Navrotsky, A. and Wood, B.J. (Eds.): *Adv. Phys. Geochem.* **Vol 1**. Springer-Verlag, Berlin, 131–147.
Ogniben, L. (1960): Nota illustrativa dello schema geologico della Sicilia nord-orientale. *Riv. Min. Sic.* **64–65**, 183–212, 2 tt., 2 ff.
Ogniben, L. (1969): Schema introduttivo alla geologia del confine calabro-lucano. *Mem. Soc. Geol. It.* **8**, 453–763.
Ogniben, L. (1973): Schema geologico della Calabria in base ai dati odierni. *Geol. Romana* **12**, 243–585.
Passchier, C.W. and Trouw, R.A.J. (1996): Microtectonics, Springer-Verlag, Berlin, 289 pp.
Perchuk, L.L. and Lavrent'eva, I.V. (1983): Experimental investigation of exchange equilibria in the system cordierite-garnet-biotite. *Advances in Physical Geochemistry* **3**. New York, Springer, 199–239.
Pezzino, A., Pannucci, S., Puglisi, G., Atzori, P., Ioppolo, S. and Lo Giudice, A. (1990): Geometry and metamorphic environment of the contact between the Aspromonte-Peloritani Unit (Upper Unit) and Madonna dei Polsi Unit (Lower Unit) in the central Aspromonte area (Calabria). *Boll. Soc. Geol. It.* **109**, 455–469.
Pezzino, A., Puglisi, G., Pannucci, S. and Ioppolo, S. (1992): Due unità cristalline a grado metamorfico diverso in Aspromonte centrale. Geometria dei loro rapporti, ambientazione metamorfica del loro contatto e caratteri petrografici delle metamorfiti. *Boll. Soc. Geol. It.* **111**, 69–80.
Platt, J.P. and Compagnoni, R. (1990): Alpine ductile deformation and metamorphism in a Calabrian basement nappe (Aspromonte, south Italy). *Ecl. Geol. Helv.* **83**, 41–58.
Powell. R. and Holland, T.J.B. (1999): Relating formulations of the thermodynamics of mineral solid solutions: activity modeling of pyroxenes, amphiboles, and micas. *Am. Mineral.* **84**, 1–14.
Pryer, L.L. (1993): Microstructures in feldspars from a major crustal thrust zone: the Greenville Front, Ontario, Canada. *J. Structural Geol.* **15**, 21–36.
Puglisi, G. and Pezzino, A. (1994): Metamorphism in the central Aspromonte area: geological, mineralogical and petrogenetic relationships. *Periodico di Mineralogia* **63**, 153–168.

Table A5 Representative analyses of feldspar.

Rock	Metapelite						Leucocratic-gneiss
Location	Southern SAC			Northern SAC	APU		
Sample	SA-11 (108)	SA-11 (148)	SA-12 (185)	SA-62 (389)	AP-2 (268)	AP-2 (292)	AP-20 (465)
Type	I	II	II	I	I	II	I
Zone	CORE	RIM	RIM	CORE	CORE	RIM	CORE
SiO_2	64.60	64.67	67.52	64.51	57.03	57.04	63.28
TiO_2	0.00	0.07	0.00	–	–	0.07	0.01
Al_2O_3	22.67	20.05	20.07	23.18	27.86	23.81	17.95
Cr_2O_3	0.00	0.33	0.06	0.10	0.13	2.16	0.00
MnO	0.00	0.00	0.02	0.02	0.00	0.05	0.02
MgO	0.00	0.08	0.00	0.00	0.01	0.75	0.01
CaO	3.63	0.63	0.05	3.96	8.77	6.17	0.05
Na_2O	9.23	11.30	12.53	9.57	6.13	6.84	0.60
K_2O	0.10	0.41	0.06	0.08	0.10	0.90	16.55
Total	100.23	97.53	100.29	101.41	100.02	97.78	98.46
Si	2.837	2.920	2.955	2.810	2.551	2.637	2.986
Al	1.174	1.066	1.034	1.189	1.468	1.296	0.998
Ti	0.000	0.002	0.000	0.000	0.000	0.003	0.000
Mg	0.000	0.005	0.000	0.000	0.001	0.052	0.000
Mn	0.000	0.000	0.001	0.000	0.000	0.002	0.001
Ca	0.171	0.030	0.002	0.185	0.420	0.306	0.002
Na	0.786	0.989	1.063	0.809	0.531	0.613	0.055
K	0.006	0.024	0.003	0.004	0.005	0.053	0.996
Ab	81.671	94.800	99.500	81.100	55.500	63.100	5.200
An	17.749	2.900	0.200	18.500	43.900	31.500	0.200
Or	0.580	2.300	0.300	0.400	0.500	5.500	94.600
Sum_cat	5.000	5.048	5.060	5.000	5.000	5.046	5.038
Sum_oxy	8	8	8	8	8	8	8

I and II: pre-mylonitic and syn- to post- mylonitic minerals, respectively

Richard, L.R. (1995): MinPet: Mineralogical and petrological data processing system, version 2.02. MinPet Geological Software, Québec, Canada

Rosenbaum, G., Lister, G.S. and Duboz, C. (2002): Relative motions of Africa, Iberia and Europe during Alpine orogeny. *Tectonophysics* **359**, 117–129.

Rosenbaum, G. and Lister, G.M. (2004): Neogene and Quaternary rollback evolution of the Tyrrhenian Sea, the Apennines, and the Sicilian Maghrebides. *Tectonics* **23**, TC1013, doi:10.1029/2003TC001518

Roser, B.P. and Korsh, R.J. (1986): Determination of tectonic Settino of sandstone-mudstone suites using SiO_2 content and K_2O/Na_2O ratio. *J. Geology* **94**, 635–650.

Rossetti, F., Faccenna, C., Goffé, B., Patrick, M., Argentieri, A., Funiciello, R. and Mattei, M. (2001): Alpine structural and metamorphic signature of the Sila Piccola Massif nappe stack (Calabria, Italy): insights for the tectonic evolution of the Calabrian Arc. *Tectonics* **20**, 112–133.

Sander, B. (1950): Einführung in die Gefügekunde der geologischen Körper, Band II: Die Korngefüge, Springer, Wien, 409 pp.

Scandone, P. (1982): Structure and evolution of the Calabrian Arc. *Earth Evol. Sci.* **3**, 172–180.

Scheepers, P.J.J. (1994): Tectonic rotations in the Tyrrhenian arc system during the Quaternary and late Tertiary. (Ph.D. thesis, Utrecht University), Geologica Ultraiectina, 112, pp. 352.

Scheepers, P.J.J., Langereis, C.G., Zijderveld, J.D.A. and Hilgen, F.J. (1994): Paleomagnetic evidence for a Pleistocene clockwise rotation of the Calabro-Peloritan block (southern Italy). *Tectonophysics* **230**, 19–48.

Schenk, V. (1980): U–Pb and Rb–Sr radiometric dates and their correlation with metamorphic events in the granulite-facies basement of the Serre, Southern Calabria, Italy. *Contr. Mineral. Petrol.* **73**, 23–38.

Stöckhert, B. and Duyster, J. (1999): Discontinuous grain growth in recrystallised vein quartz – implications for grain boundary structure, grain boundary mobility, crystallographic preferred orientation, and stress history. *J. Structural Geol.* **21**, 1477–1490.

Tortorici, L. (1983): Lineamenti geologico-strutturali dell'Arco Calabro. *Rend. Soc. It. Min. Pet.* **38**, 927–940.

Van Dijk, J.P., Bello, M., Brancaleoni, G.P., Cantarella, G., Costa, V., Frixa, A., Golfetto, F., Merlini, S., Riva,

Table A6 Representative analyses of epidote and amphibole.

Mineral	Epidote		Amphibole			
Rock	Metapelite		Amphibole-bearing schist			
Location	Southern SAC	APU	Northern SAC		APU	
Sample	SA-12 (196)	AP-2 (221)	SA-58 (237)	SA-58 (250)	AP-12 (5)	AP-13 (18)
Type	II	II	I	I	I	II
Zone	CORE	CORE	CORE	RIM	CORE	CORE
SiO_2	38.64	38.07	55.32	43.08	46.67	41.06
TiO_2	0.18	0	0.23	0.36	0.62	0.23
Al_2O_3	24.94	24.97	16.66	16.47	10.01	17.27
FeO^{tot}	–	–	8.68	16.57	14.12	19.05
$Fe_2O_3^{tot}$	9.54	11.64				
Cr_2O_3	0	0	0.05	0.03	0.04	0.00
MnO	0.17	0	0.09	0.06	0.25	0.24
MgO	0.08	0	3.63	8.53	12.62	6.73
CaO	21.22	24.35	4.86	9.88	12.07	10.09
Na_2O	0.76	0	8.01	2.33	1.31	2.27
K_2O	0.46	0	0.16	0.48	0.33	0.51
Total	95.99	99.03	97.69	97.79	98.04	97.45
Si	3.087	2.983	7.638	6.184	6.757	6.083
Al^{IV}	0	0.017	0.362	1.816	1.243	1.917
Al^{VI}	2.347	2.287	2.347	0.968	0.465	1.098
Cr	0	0	0.005	0.003	0.005	0.000
Fe^2	–	–	0.925	0.661	1.244	1.500
Fe^3	0.573	0.686	0.078	1.328	0.466	0.816
Ti	0.011	0	0.024	0.039	0.068	0.026
Mg	0.01	0	0.747	1.825	2.723	1.486
Mn	0.012	0	0.011	0.007	0.031	0.030
Ca	1.817	2.044	0.719	1.519	1.872	1.601
Na_{M4}	–	–	2.000	0.649	0.128	0.399
Na_A	–	–	0.144	0.000	0.240	0.253
Na_{tot}	0.118	0	2.144	0.649	0.368	0.652
K	0.047	0	0.028	0.088	0.061	0.096
Sum_oxy	12.5	12.5	23	23	23	23

I and II: pre-mylonitic and syn- to post- mylonitic minerals, respectively.

M., Torricelli, S., Toscano, C. and Zerilli, A. (2000): A regional structural model for the northern sector of the Calabrian Arc (southern Italy). *Tectonophysics* **324**, 267–320.

Worley, B. and Powell R. (1998): Singularities in NCKF-MASH (Na_2O–CaO–K_2O–FeO–MgO–$AL_2O_3SiO_2$–H_2O). *J. Metamorphic Geol.* **12**, 99–119.

Received 3 January 2005
Accepted in revised form 25 July 2005
Editorial handling: M. Engi.

Appendix 1

Analytical conditions and representative analyses

Bulk composition was obtained by XRF on a Philips PW 2404 spectrometer of the Department of Geological Sciences, University of Catania. Mineral composition was measured at Department of Earth Sciences, University of Modena, on an ARL-SEMQ microprobe. Operating conditions for microprobe analyses: 15 kV and 15 nA; integration time 10 s; natural and synthetic pure oxides used as standards for calibration. A PAP program was used to convert counts into wt% of oxides. Mineral formulae and ferric/ferrous iron ratios calculated using MINPET 2.02 program (Richard, 1995), on the basis of 12 oxygens and 8 cations for garnet, 23 oxygens and average Fe^{3+} (cation sum – K=15) for amphibole, 11 oxygens for micas, 28 oxygens for chlorites; for epidote, all Fe content was considered Fe^{3+}.

Appendix 2

Mineral solid solution model

Solid solution models are: Chlorite – non-ideal model for clinochlore, daphnite, amesite, ferroamesite, Al-free chlorite and Fe-Al-free chlorite (*Holland* and *Powell*, 1998); Biotite – Fe-Mg-Mn biotite (*Powell* and *Holland*, 1999); Plagioclase 1 – model for albite-rich side of plagioclase solid solution (*Newton* and *Haselton*, 1981); Plagioclase 2 – ideal ternary feldspar (*Furman* and *Lindsley*, 1988); White mica – potassium phengitic mica encompassing paragonite-celadonite-ferroceladonite-muscovite (*Holland* et al., 1998); Garnet – quaternary garnet model among grossular, pyrope, almandine, spessartine (*Holland* and *Powell*, 1998) and Epidote – non-ideal mixing model for clinozoisite, ferro-epidote end-members (*Holland* and *Powell*, 1998). Above solution model is in agreement with *Connolly* and *Petrini* (2002).